Neural Field Model of VSD Optical Imaging Signals

François Grimbert, Frédéric Chavane

INSTITUT NATIONAL DE RECHERCHE EN INFORMATIQUE ET EN AUTOMATIQUE

Neural Field Model of VSD Optical Imaging Signals

François Grimbert — Frédéric Chavane

N° 6398

December 2007

Thème BIO

ISSN 0249-6399 ISRN INRIA/RR--6398--FR+ENG

Neural Field Model of VSD Optical Imaging Signals

François Grimbert*, Frédéric Chavane†

Thème BIO — Systèmes biologiques
Projet Odyssée

Rapport de recherche n° 6398 — December 2007 — 46 pages

Abstract: In this report we propose a solution to the direct problem of VSD optical imaging based on a neural field model of a cortical area and reproduce optical signals observed in various mammals cortices. We first present a biophysical approach to neural fields and show that these easily integrate the biological knowledge on cortical structure, especially horizontal and vertical connectivity patterns. After having introduced the reader to VSD optical imaging, we propose a biophysical formula expressing the optical imaging signal in terms of the activity of the field. Then, we simulate optical signals that have been observed by experimentalists. We have chosen two experimental sets: the line-motion illusion in the visual cortex of mammals [15] and the spread of activity in the rat barrel cortex [23]. We begin with a structural description of both areas, with a focus on horizontal connectivity. Finally we simulate the corresponding neural field equations and extract the optical signal using the direct problem formula developed in the preceding sections. We have been able to reproduce the main experimental results with these models.

Key-words: neural field, biophysical model, optical imaging, direct problem, connectivity, visual cortex, barrel cortex

This work was partially supported by Elekta AB.

* INRIA Sophia-Antipolis, Projet Odyssée
† Institut de Neurosciences Cognitives de la Méditerrannée, Marseille

Unité de recherche INRIA Sophia Antipolis
2004, route des Lucioles, BP 93, 06902 Sophia Antipolis Cedex (France)
Téléphone : +33 4 92 38 77 77 — Télécopie : +33 4 92 38 77 65

Modèle du signal d'imagerie optique extrinsèque basé sur un champ neuronal

Résumé : Dans ce rapport, nous proposons une solution au problème direct de l'imagerie optique extrinsèque basée sur un modèle de champ neuronal d'une aire corticale et nous reproduisons des signaux optiques observés dans plusieurs cortex chez le mammifère. En premier lieu, nous présentons une approche biophysique des champs neuronaux et nous montrons que ceux-ci intègrent aisément les connaissances biologiques sur la structure du cortex, en particulier les connectivités horizontales et verticales. Après avoir présenté au lecteur les principes de l'imagerie optique, nous proposons une formule biophysique exprimant le signal optique en fonction de l'activité du champ. Ensuite, nous simulons des signaux optiques qui ont été observés par des expérimentalistes. Nous avons choisi deux expériences: l'illusion de mouvement dans le cortex visuel des mammifères [15] et la propagation de l'activité dans le cortex tonnelé du rat [23]. Nous commençons par une description structurelle de ces deux aires en nous concentrant sur les connectivités. Pour finir, nous simulons les équations de champ neuronal correspondantes et nous extrayons le signal optique en utilisant la formule du problème direct développée dans les sections précédentes. Nous avons ainsi été capables de reproduire les principaux résultats expérimentaux à l'aide de ces modèles.

Mots-clés : champ neuronal, modèle biophysique, imagerie optique, problème direct, connectivité, cortex visuel, cortex tonnelé

Contents

1 Neural field model of a cortical area

In mammals brain, gray matter (intracortical) projections almost exclusively connect neurons within the same area and white matter projections mostly connect neurons from different areas [25]. In the following, we will see a cortical area as an autonomous intracortical network, described by a neural field equation, including several layers and receiving distributed sensory input from white matter afferents (see figure 1).

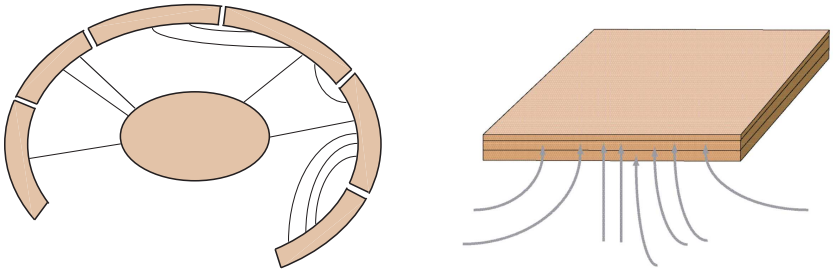

Figure 1: *Left. Simplified representation of the brain that we assume in our modeling of a cortical area: areas are defined as autonomous structures receiving input from other parts of the brain. The central ovoid form represents the thalamus, the other brown regions being cortical areas. Black curves account for white matter connections. Right. Focus on a single area. We see it as a layered intracortical network receiving sensory input via white matter projections.*

In this section, we want to show that neural field models parameters and variables can naturally be related to well-known biological facts.

We start from classical neural field models and analyze them from a biophysical viewpoint.

$$\dot{\mathbf{V}}(\mathbf{r},t) = -\mathbf{L}\mathbf{V}(\mathbf{r},t) + \int_{\Omega} \mathbf{W}(\mathbf{r},\mathbf{r}')\mathbf{S}(\mathbf{V}(\mathbf{r}',t))\,d\mathbf{r}' + \mathbf{I}_{\text{ext}}(\mathbf{r},t), \tag{1}$$

and

$$\dot{\mathbf{A}}(\mathbf{r},t) = -\mathbf{L}\mathbf{A}(\mathbf{r},t) + \mathbf{S}\left(\int_{\Omega} \mathbf{W}(\mathbf{r},\mathbf{r}')\mathbf{A}(\mathbf{r}',t))\,d\mathbf{r}' + \mathbf{I}_{\text{ext}}(\mathbf{r},t)\right). \tag{2}$$

Ω is the spatial domain defining the area, a compact subdomain of $\mathbb{R}^2$ (e.g. a square or a disk). For each spatial position $\mathbf{r} \in \Omega$, the underlying cortical column is described, at time t, by an N-dimensional vector $\mathbf{V}(\mathbf{r},t)$ or $\mathbf{A}(\mathbf{r},t)$. $\mathbf{V}(\mathbf{r},t)$ contains the average soma membrane potentials of the different neural masses present in the column. So, N is the number of neuronal types considered in every column. Each neuronal type can be thought of as belonging to a particular cortical layer, the layer the corresponding somata belong to. $\mathbf{A}(\mathbf{r},t)$ contains the average activities of the masses.

$$A_i = PSP_i * \nu_i,$$

where $*$ represents the temporal convolution, ν_i the average firing rate of mass i and PSP_i the normalized[1] postsynaptic potential induced by mass i on its postsynaptic targets. So A_i is the potential quantity of post-synaptic potential induced by mass i on the dendrites of all its postsynaptic partners. The actual quantity depends on the strength and sign (excitatory or inhibitory) of the projections.
Here it is assumed that postsynaptic potentials have a decreasing exponential form, completely characterized by their time constant (up to the sign and intensity of connections, see figure 2):

$$PSP_i(t) = \begin{cases} e^{-t/\tau_i}, & t > 0 \\ 0, & t \leq 0 \end{cases} .$$

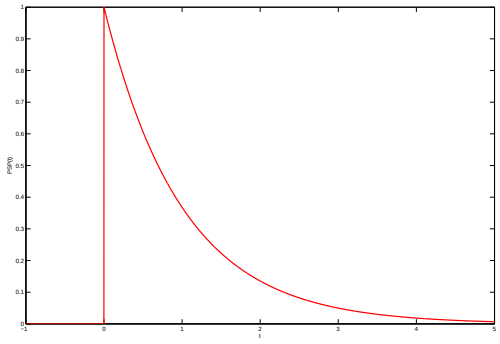

Figure 2: *Form of a normalized postsynaptic potential that we assume in our models. As τ gets bigger, PSP gets broader.*

$\mathbf{L}$ is an $N \times N$ diagonal matrix containing the synaptic decay time constants τ_i of the postsynaptic potentials $PSP_i(t)$ for the different neuronal types. As we have seen before, in the voltage case, the time constants only depend on the postsynaptic population, while in the activity case they only depend on the presynaptic one. In real neurons these constants actually depend on both populations and on their current electrophysiological state (in terms of ionic channels openings), what allows to explain such phenomena as shunting inhibition. However among the two presented models, the activity-based model is the most realistic. Indeed, the characteristic time constant of a postsynaptic potential more likely depends on the neurotransmitter that triggered it, and so, on the presynaptic neuron.
$\mathbf{I}_{\text{ext}}(\mathbf{r}, t)$ is an input term to the system, corresponding to projections that arise from white matter. For example in V1, it would correspond to the input from the lateral geniculate

[1] *Normalized* in the sense that it does not include the strength and sign of connections from mass i to its postsynaptic partner.

nucleus (LGN, the thalamic relay from the retina to the cortex) and feedbacks from the secondary visual cortex, V2 (see figure 3).

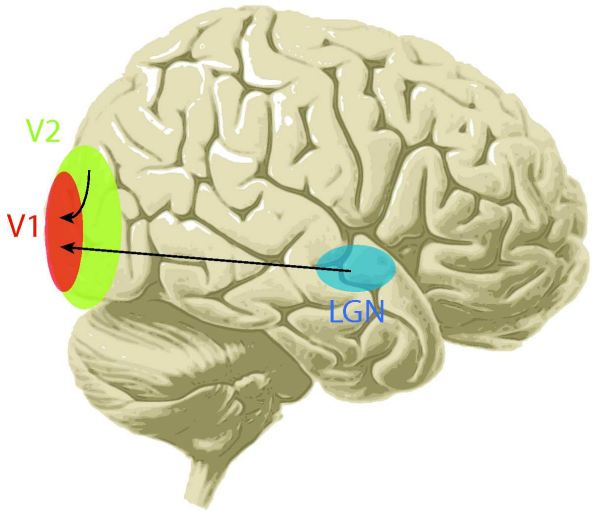

Figure 3: *External inputs to V1, arising from white matter fibers: feedforward projections from the LGN and feedback projections from V2.*

The input can be seen as a current (voltage case) or an electric potential (activity case) on the dendrites of thalamo-recipient cells. The main problem concerning the input term is that few is currently known about the coding of sensory information by sensory organs and their thalamic relays to the cortex.

In equations (1) and (2), the integral terms summate the contributions from columns at different locations on the field to the dynamics of the column located at point $\mathbf{r}$. They feature an intracortical connectivity kernel $\mathbf{W}$ representing the weights of connections between columns located at different positions on the field and a nonlinear function $\mathbf{S} : \mathbb{R}^N \rightarrow \mathbb{R}^N$. $\mathbf{S}$ has N components. Each of them is a static sigmoidal (nonlinear) transformation converting, for a given neuronal type, the average soma potential of a neural mass into its average firing rate. This sigmoidal shape (see figure 4) is in agreement with studies made by Walter Freeman in the olfactory bulb.
He showed that the mapping between the average membrane potential of a neural mass and its average firing rate was a sigmoidal "wave-to-pulse" transform, by comparing the amplitude of EEG signals produced by neural masses with their firing probabilities [10]. The abscissa of the sigmoid's inflection point can be thought of as the average excitability or firing threshold of the corresponding neuronal population, and the limit of the sigmoid at

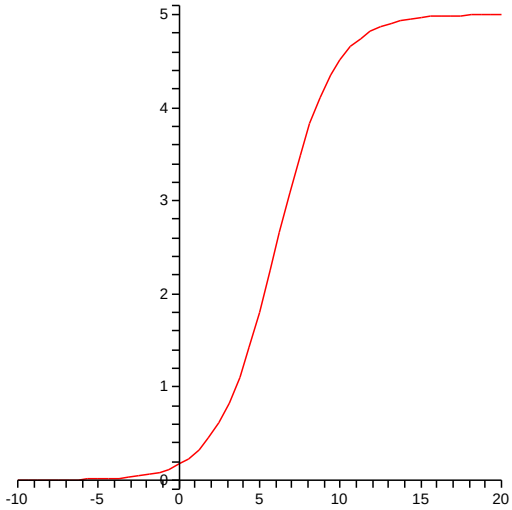

Figure 4: *Function Sigm used in this model. It converts the average membrane potential of a mass into its average firing rate.*

infinity, as its maximal firing rate.

$\mathbf{W}$ is an $N \times N$ matrix. The terms W_{ij} represent the strength of projections from neurons of type j to neurons of type i. But what does "strength" mean? Each connectivity term can be seen as the product of three quantities:

$$W_{ij} = N_j \, k_{ij} \, w_{ij},$$

where N_j is the number of neurons of type j in one column, k_{ij} the gain of an average postsynaptic potential caused by a neuron of type j on a neuron of type i, and w_{ij}, the average number of synaptic contacts that a neuron of type j makes on a neuron of type i. It can also be seen as the probability of synaptic contact between the axon of a neuron of type j and the postsynaptic compartments of a neuron of type i.
So in first approximation we can think of $\mathbf{W}$ as a wiring diagram such as the one shown in figure 5, where the matrix components W_{ij} are represented by arrows linking neuronal types.
However, a diagram such as figure 5 only provides information on the "vertical" intracolumnar connectivity between neural masses. Horizontal intercolumnar connections are also included in $\mathbf{W}$. Each W_{ij} is actually a function depending on two positions on the field and $W_{ij}(\mathbf{r}, \mathbf{r}')$ indicates the strength of projections from the mass of type j, in column $\mathbf{r}'$ to the mass of type i, in column $\mathbf{r}$. The vertical connectivity information for column $\mathbf{r}$ can be found in $\mathbf{W}(\mathbf{r}, \mathbf{r})$. $W_{ij}(\cdot, \mathbf{r}')$ is the spatial horizontal distribution of projections from the mass $(j, \mathbf{r}')$ to masses of type i, which depends on the horizontal spread of both the axonal arborization of mass $(j, \mathbf{r}')$ and the dendrites of masses of type i (see figure 6).
Horizontal connectivity patterns play a major functional role and widely vary from an area to another. We will see examples of these patterns in the following for two different cortices: the primary visual cortex of a wide range of mammals and the rat barrel cortex.

So, we have seen that neural fields can be suitable mesoscopic models of cortical areas. Their parameters can be tuned in agreement with well-known biophysical quantities and account for the complex structure of an area in terms of layers, horizontal and vertical connectivity. In the following we will focus on the activity-based model, because it is more realistic than the voltage-based model as concerns synaptic integration and facilitate the description of the optical imaging signals that we will propose later.

2 Principle of VSD optical imaging

VSD optical imaging[2] (VSDOI) is a recent and popular functional imaging technique that uses fluorescent voltage sensitive dyes (VSD) to reveal population activity of cortical neurons in behaving animals [12], with high spatial resolution ($\sim 0.5\mu$m for single cell recordings and $\sim 50\mu$m for population recordings) and a temporal precision inferior to the millisecond. This

[2] Also known as *extrinsic optical imaging*.

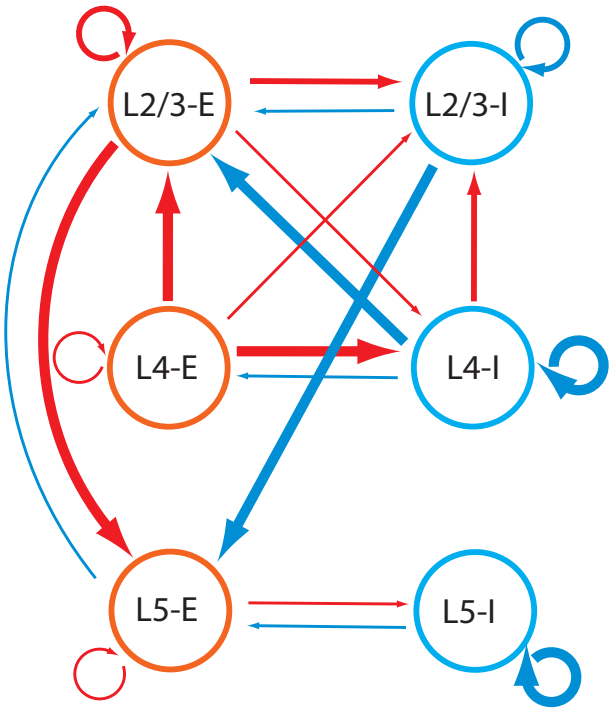

Figure 5: *A example of simplified model of cortical interactions based on six neuronal populations. It features three layers corresponding to cortical layers II/III, IV and V, and two types of neurons (excitatory ones in red and inhibitory ones in blue). The size of the arrows gives an idea of the strength of the connectivity between populations (adapted from [13]).*

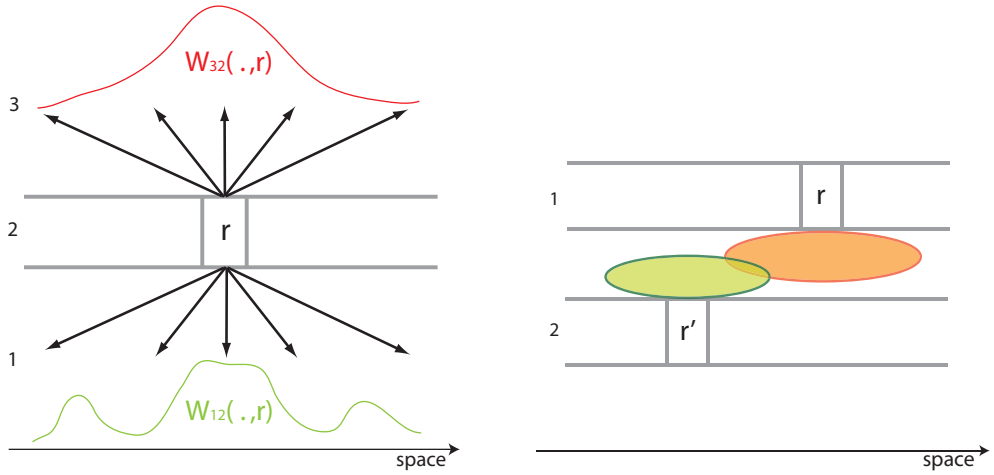

Figure 6: *Left. Example featuring three neuronal types (1, 2 and 3). The mass* $(2, \mathbf{r})$ *shows different spatial patterns of horizontal projections, depending on the type of the postsynaptic targets. Right. The axonal arbour of mass* $(1, \mathbf{r})$ *(in red) does not reach* $\mathbf{r}'$ *but since the dendritic tree of* $(2, \mathbf{r}')$ *(in green) is wide enough,* $W_{21}(\mathbf{r}', \mathbf{r}) \neq 0$.

invasive technique requires an opening in the skull to have direct access to the cortex (see figure 7, lower panel). Hence, it has mostly been used in non-human mammals, like monkeys, cats and rodents.
As the cortex is stained with VSD, the dye molecules bind to the plasmic membrane of all types of cells present in the cortex. These include glial cells and all compartments of neurons. VSD molecules are polarized, because of the electric potential at the level of neurons membranes, and emit light with an intensity proportional to this polarization (see figure 7, upper right panel). Glial cells are known to have a minimal contribution to VSD signals because of their lower electrical activity compared to neurons. So light patterns emitted from the cortex and recorded by the camera of the optical imaging device (figure 7, upper left panel) are mostly due to the electrical activity of neurons. VSDOI signals show a remarkable match with intracellular recordings. Actually, at the level of a single cell, the amplitude of VSD signals is linearly correlated with both the membrane potential and the area of stained neuronal membranes. In neuronal population imaging, a pixel contains the blurred images of various neuronal compartments. How strongly do the different compartments contribute to the VSD signal? The surface of somata is several orders of magnitude smaller than the surface of axons and dendrites. So somata make a minor contribution to the VSD signal. Dendrites are more confined, horizontally, than axonal arbours, and spikes traveling down the axons are too brief events to be well integrated in the population VSD signal. So, the optical signal is mainly due to the subthreshold, dendritic activity of the underlying

population of neurons (see the comparison of the optical signal with an intracellular recording on figure 7).

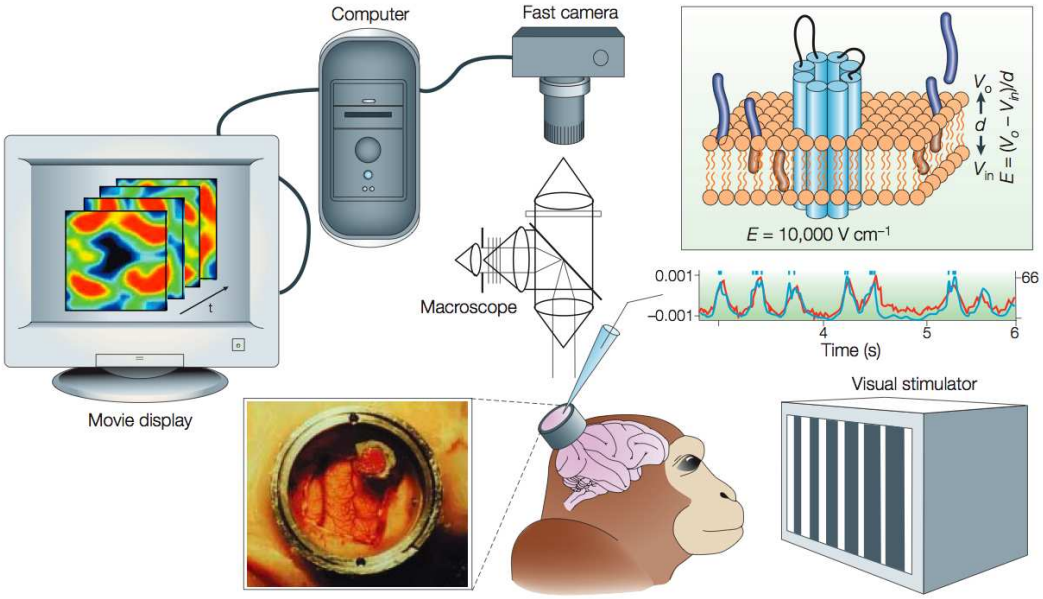

Figure 7: *Principle of VSDOI. An opening in the skull of a behaving monkey gives access to its cortex stained with VSD. A camera records the fluorescence caused by polarized VSD molecules bound to the plasmic membrane of cortical neurons, and after appropriate processing, a movie of the distributed population activity is obtained, with high spatial and temporal resolutions. The optical signal (in red on the right central panel) remarkably matches the subthreshold dynamics of neurons obtained by intracellular recordings (in blue; truncated spikes are represented by small blue dots overlying the subthreshold signal) (From [12]).*

The integration of the optical signal across the depth of the cortex is subject to a double gradient. First, VSD molecules mostly diffuse in the superficial layers and few of them deeply penetrate the cortex. In [21], the authors show that most of the dye molecules[3] lie in layers I-III (70%) (see figure 8).
Second, the light emitted by deep VSD molecules undergoes stronger diffusive effects, traveling back to the surface across cortical cells. Hence activity in layers IV-VI poorly contribution to the signal.

[3]They used the blue dye RH1691, developed by Amiram Grinvald's group, in the cortex of the rat.

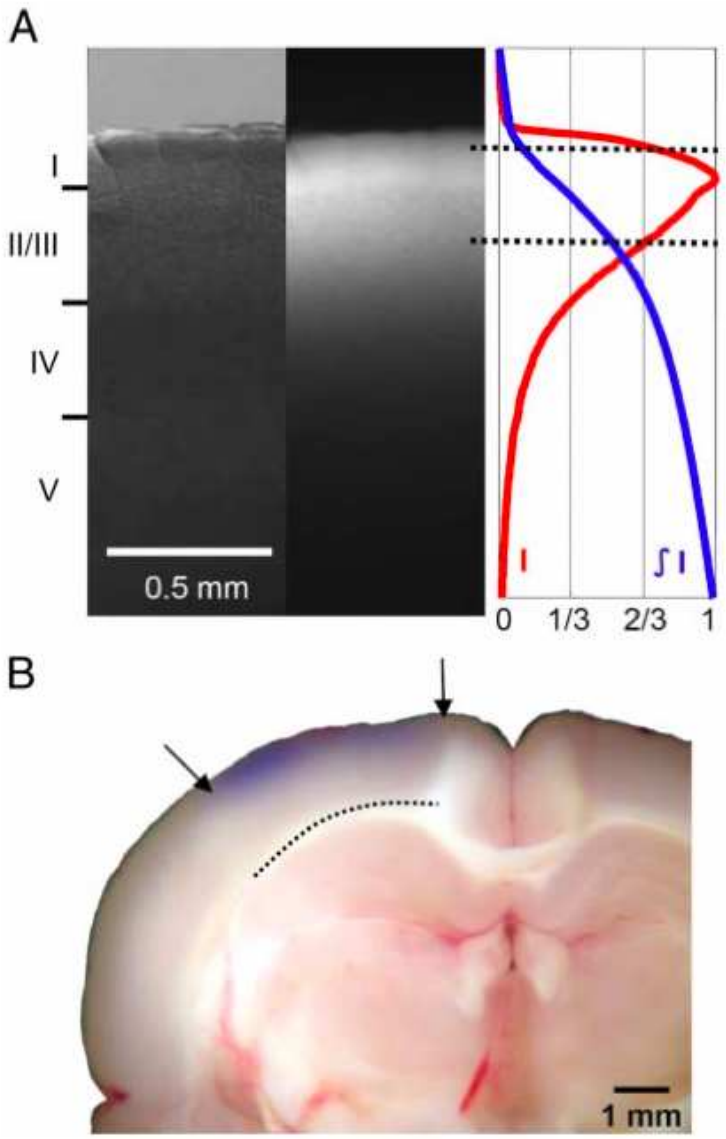

Figure 8: *A. Left. Visible light image of a stained cortical slice. Middle. Corresponding fluorescence image showing the density distribution of VSD molecules across the layers. Right. Corresponding fluorescence intensity (red) and intergrated intensity (blue). We observe that about 30% of the staining dye molecules are located in layer I and about 70% in layers I-III. B. Stained brain section. Arrows indicate the borders of the previously opened cranial window. Broken line indicates the border between gray and white matter. The staining can be seen by eye in blue (From [21]).*

We now propose a model for VSDOI signals produced by a cortical area, grounded in the above facts, and based on a neural field description of the spatially distributed activity of neural masses in the area.

3 Model of the OI signal

In this section we write a formula involving the variables and parameters of a neural field model to solve the direct problem of VSDOI.
To that purpose we start from the whole signal and decompose it, step by step, into elementary contributors until we reach the cellular membrane level, where the optical signal is simply proportional to the membrane potential. Firstly, the signal is a weighted sum of the signals arising from the different layers. We term the whole signal as OI, and the unattenuated signal from layer l as OI^l. Here, "unattenuated" means that we suppose that no superimposed layer would hamper the propagation of light towards the camera. We then have the following

$$OI(\mathbf{r},t) = \sum_{l\in\{\text{layers}\}} a_l\, OI^l(\mathbf{r},t),$$

where a_l is a positive attenuation coefficient due absorption and diffusion of the light emitted by layer l through its superimposed layers. Naturally, a_l decreases as the depth of the layer increases. Then it is natural to sum these attenuated light contributions in virtue of the linearity of Maxwell equations.
The propagation of light through the cortical tissue is not well-known, but diffusion and absorption of light by gray matter probably would be more suitably modeled by a spatial blurring of the signals produced by a layer. Hence the previous formula would become

$$OI(\mathbf{r},t) = \sum_{l\in\{\text{layers}\}} a_l\, G_l \otimes OI^l(\mathbf{r},t),$$

where G_l is a two-dimensional Gaussian distribution whose standard deviation increases with the depth of layer l, and $\otimes$ denotes the spatial convolution (see figure 9).
Now, what is the local instantaneous quantity of light $OI^l(\mathbf{r},t)$ produced by layer l?

$$OI^l = \sum_{i=1}^{N} OI^l_i,$$

where N is the number of neuronal types considered in the neural field and OI^l_i the contribution of dendrites belonging to neurons of type i and lying in layer l[4] to the unattenuated layer signal (see figure 10).

[4]From now on, we will designate dendritic trees by a doublet (l,i) indicating the layer and the neuronal type it belongs to.

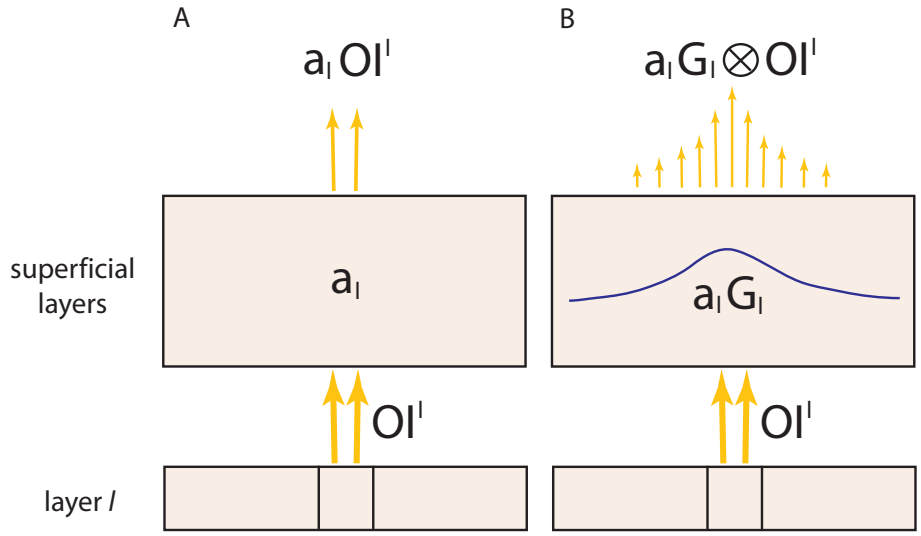

Figure 9: *Two models of light absorption/diffusion in superficial layers. A. The fluorescence produced in layer l at the level of one neural mass is simply attenuated by absorption in superficial layers, keeping its initial spatial focus. B. In this model, the same focused emission of light in layer l is attenuated by absorption and horizontally diffused by multiple scattering in the cortical cellular network. This phenomenon can be accounted for by a convolution of the signal with a Gaussian distribution. It results, at the exit of the cortex, in a blurred emission of light.*

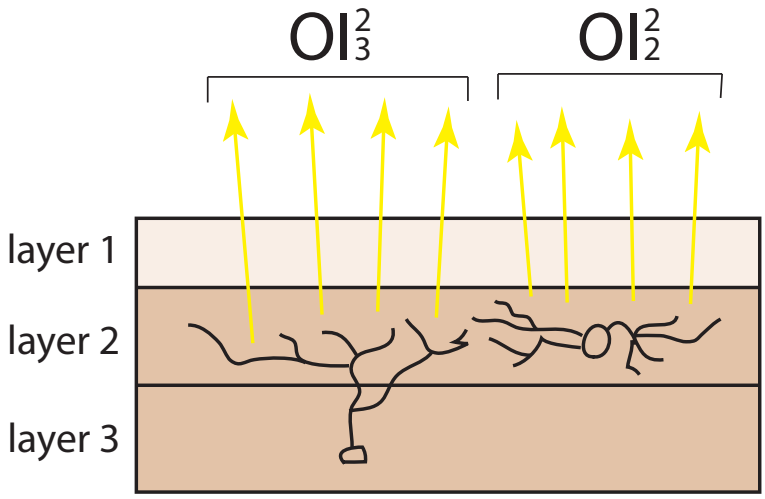

Figure 10: *The emission of light at the level of a layer (here layer 2), forgetting the attenuation due to superimposed layers (like layer 1, in light color), is the sum of the contributions from neurons which project part of their dendritic trees in the emitting layer, no matter where their somata are located.*

Note that the somata of neurons of type i do not need lie in layer l so that part of their dendritic trees do, and hence contribute to the layer signal. For example deep layers pyramidal cells have several dendritic arbors and some of them reach the most superficial cortical layers (see figure 11).
Now we focus on $OI^l_i(\mathbf{r},t)$, the local unattenuated contribution of the dendritic tree (l,i).

$$OI^l_i(\mathbf{r},t) = c\, N_i\, s^l_i\, n_l\, P^l_i(\mathbf{r},t),$$

where P^l_i is the membrane potential of (l,i), n_l the number of VSD molecules per membrane surface unit in layer l, s^l_i the average dendritic surface due to one neuron of type i in layer l and N_i the number of neurons of type i in a cortical column. So, $N_i\, s^l_i\, n_l$ is the total number of dye molecules, in the extent of one cortical column, on the dendritic tree (l,i). Finally, c is the coefficient of the linear transformation converting the local membrane potential into the optical imaging signal (see figure 12).
Now, how can we express the dendritic membrane potentials $P^l_i(\mathbf{r},t)$ in a model without any specific attention paid to neuronal compartments and where a neural mass is a simple point of the field?
Instead of trying to infer the dendritic potential $P^l_i(\mathbf{r},t)$ from the knowledge of the activity vector of column $\mathbf{r}$, $\mathbf{A}(\mathbf{r},t)$, we consider all projections to column $\mathbf{r}$. We note $PSP^l_{ij}(\mathbf{r},t)$ the total postsynaptic potential caused at time t on the dendritic tree (l,i) of column $\mathbf{r}$ by

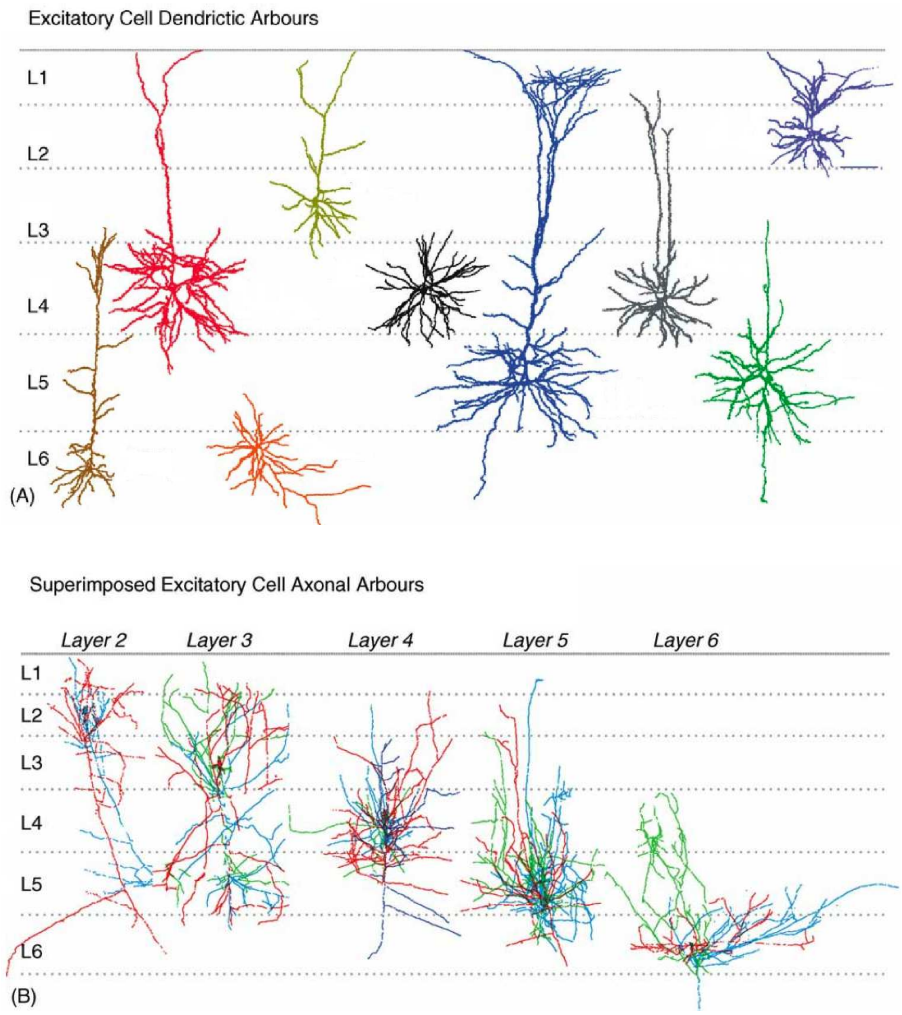

Figure 11: *Dendritic arbors (upper panel) and axonal trees (lower panel) of excitatory neurons. In the lower panel, the different axonal trees belonging to the same neuron are distinguished by different colors (From [3]).*

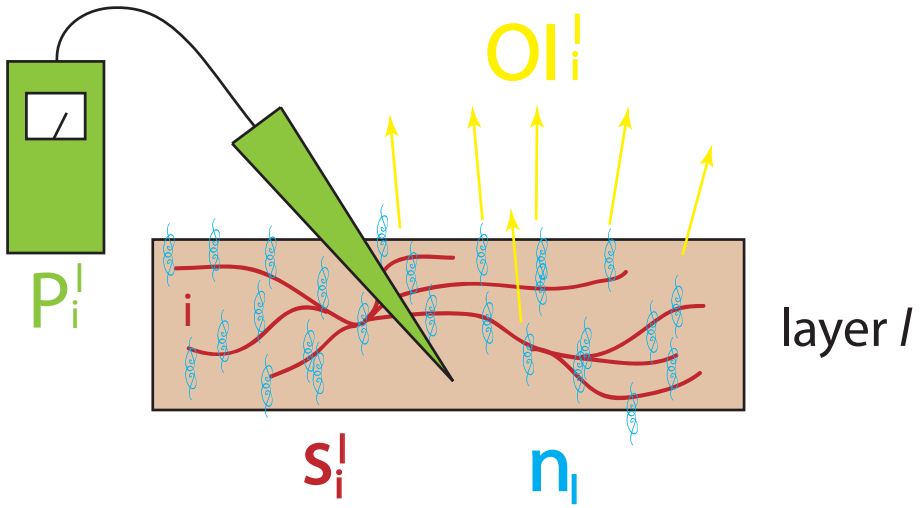

Figure 12: *The optical imaging signal (yellow) is locally linearly correlated to the dendritic membrane potential (green), the concentration of VSD molecules (blue) and the dendritic surface (red).*

all masses of type j across the area. Then assuming a linear summation of postsynaptic potentials as we did in neural field models, we have

$$P_i^l(\mathbf{r},t) = \sum_{j=1}^{N} PSP_{ij}^l(\mathbf{r},t),$$

with

$$PSP_{ij}^l(\mathbf{r},t) = \alpha_{ij}^l \int_\Omega W_{ij}(\mathbf{r},\mathbf{r}')\, A_j(\mathbf{r}',t)\, d\mathbf{r}'.$$

$\alpha_{ij}^l \in [0,1]$ is the fraction of synapses masses of type j make on dendrites of type i at the level of layer l, i.e. the number of synapses made by neurons of type j on (l,i) divided by the total number of synapses made by neurons of type j on neurons of type i[5]. Hence in general $\sum_l \alpha_{ij}^l \leq 1$. If neurons of type j exclusively target dendrites, then $\sum_l \alpha_{ij}^l = 1$. If in the opposite case they only target somata, $\sum_l \alpha_{ij}^l = 0$.

Now, we are ready to summate all elementary terms to obtain a formula for the direct problem of VSDOI:

$$OI(\mathbf{r},t) = \sum_{i,j=1}^{N} C_{ij} \int_\Omega w_{ij}(\mathbf{r},\mathbf{r}')\, A_j(\mathbf{r}',t)\, d\mathbf{r}', \tag{3}$$

with

$$C_{ij} = c\, N_i\, N_j\, k_{ij} \sum_{l\in\{\text{layers}\}} s_i^l\, \alpha_{ij}^l\, a_l\, n_l.$$

If we assume a more realistic, Gaussian diffusion, we have

$$OI(\cdot,t) = \sum_{i,j=1}^{N} C_{ij} \otimes \int_\Omega w_{ij}(\cdot,\mathbf{r}')\, A_j(\mathbf{r}',t)\, d\mathbf{r}', \tag{4}$$

with

$$C_{ij} = c\, N_i\, N_j\, k_{ij} \sum_{l\in\{\text{layers}\}} s_i^l\, \alpha_{ij}^l\, n_l\, a_l\, G_l.$$

Formulas (3) and (4) are equivalent to

$$OI(\mathbf{r},t) = \sum_{j=1}^{N} \int_\Omega \tilde{w}_j(\mathbf{r},\mathbf{r}')\, A_j(\mathbf{r}',t)\, d\mathbf{r}', \tag{5}$$

with

$$\tilde{w}_j(\mathbf{r},\mathbf{r}') = \sum_{i=1}^{N} C_{ij}\, w_{ij}(\mathbf{r},\mathbf{r}'),$$

[5]Here we implicitly assumed, for simplicity, that α_{ij}^l does not depend on the relative horizontal position of masses.

or

$$\tilde{w}_j(\mathbf{r},\mathbf{r}') = \sum_{i=1}^{N} \int_{\Omega} C_{ij}(\mathbf{r}-\mathbf{r}'')\, w_{ij}(\mathbf{r}'',\mathbf{r}')\, d\mathbf{r}''.$$

We see from (3), (4) and (5) that the horizontal distribution patterns of intracortical connectivity play a primary role in shaping the optical signal.

So, assuming a linear summation of postsynaptic potentials on cellular membranes, we have expressed the direct problem of VSDOI as a time-invariant linear operator providing at each time instant the instantaneous optical signal from the knowledge of the instantaneous activity of the field. If we note this operator $\mathbf{T}$, formulas (3), (4) and (5) reduce to

$$OI(\cdot,t) = \mathbf{T}\,\mathbf{A}(\cdot,t), \quad \forall t \geq 0.$$

Moreover, $\mathbf{T} : \mathrm{L}^2(\Omega,\mathbb{R}^N) \rightarrow \mathrm{L}^2(\Omega,\mathbb{R})$ is obviously compact, as a sum of Hilbert-Schmidt operators.
As concerns the inverse problem, it is most probably ill-posed (due to the higher dimensionality of the activity space compared to the signal space) and is not treated here.
Now that we have a model of cortical activity and a formula for VSDOI signals, we are ready to apply them to the simulation of real optical imaging experiments.

In the following, we try to reproduce the results of optical imaging experimental paradigms found in the literature, by simulating adequate neural fields and extracting the optical signals thanks to the formula we just developed. We have seen that horizontal connectivity patterns play a major role in shaping VSDOI signals. So, we start with a description of the horizontal connectivity of both cortices we focus on: the primary visual cortex and the barrel cortex. Then, we include the main features of these connectivities in neural field models and perform simulations.

4 Horizontal connectivity

Horizontal trans-columnar connectivity has an important functional role in the cortex and expresses through different arborization patterns. Though, two features must be retained as fundamental: a strong intracolumnar connectivity and a global horizontal decrease of connection intensity with the distance separating neural masses.
Neurons axonal trees ramify horizontally and connect to more or less distant post-synaptic targets. Axon collaterals (branches of the axonal tree emerging from the main axon of a neuron) can even make intracortical horizontal projections up to several millimeters. Most interneurones (including spiny stellate cells) essentially make local projections in their column of origin, while pyramidal cells and large basket cells also form extensive trans-columnar projections. The connection strength between two neurons generally decreases with the distance separating the somata. However, strong selective long-range projections, called *patches*, may exist in certain cortices.

Two particular structures have received considerable attention from neuroscientists: the lateral distribution of connections in mammals visual cortex [8, 18, 19, 20, 28, 29, 30] and the barrel organization of rats sensory cortex [2, 7, 9, 11, 22, 26, 27].

4.1 Mammals visual cortex

The primary visual of certain mammals (including monkeys and cats, but not rats) can be divided into orientation preference columns [14]. This means that cortical columns in the visual cortex preferentially respond to certain oriented visual stimuli (vertical, horizontal, oblique bars). So, each column can be labeled with a preferred orientation and orientation preference maps of the visual cortex can be reconstructed thanks to different functional imaging techniques (see figure 13).
The main feature of horizontal connectivity in the primary visual areas of such mammals is the patchy, orientation-preference-biased structure of pyramidal cells long-range projections (see figures 14 and 15).
In [8], the authors examine the relationship between excitatory lateral connections and orientation maps in the cat primary visual cortex. Thanks to tracer injections they were able to track the axonal projections issued from a small cortical site. They showed that most proximal projections do not discriminate their target in terms of orientation preference while distal patches usually do (figure 15). Actually, the regions underlying distal patches tend to have the same orientation preference as the region from which the projections originate. This tendency, which has been observed for projections originating from a localized cluster of cells (i.e. a neural mass), is however not clear when tracking the targets of single cells. Indeed their long-range projections are not necessarily patchy nor orientation selective (see figure 16).
So, patchy functional projections made by PC clusters are consistent with our mesoscopic neural mass approach, but they are too coarse to embrace the complexity of the precise functional network.
One last striking feature in PCs long-range projections is the anisotropy observed in the spatial distribution of patches. It appears that the main direction of this distribution is orthogonal to the preferred orientation of the injected site (see figure 15).

Large basket cells also make trans-columnar projections, up to one or two millimeters, but these are not patchy and have a lesser, 2-3 times smaller spatial extent than projections from excitatory cells (see figure 17) [20].
However, these projections show distance-dependent selectivity according to orientation as well as direction preference. In [19] the authors observe that specificity expresses in two features of the axonal arbour of a large basket cell. The proximal and distal parts of the arbour have distinct orientation and direction selectivities. While local projections show similar preferences to that of the parent soma, distal ones terminate most frequently in regions of non-preferred orientation and opposite preferred direction. Moreover, the axonal arbour of large basket cells can be dissected into two main trees bifurcating near the soma of the cell, which show different orientation selectivity in their distal parts.

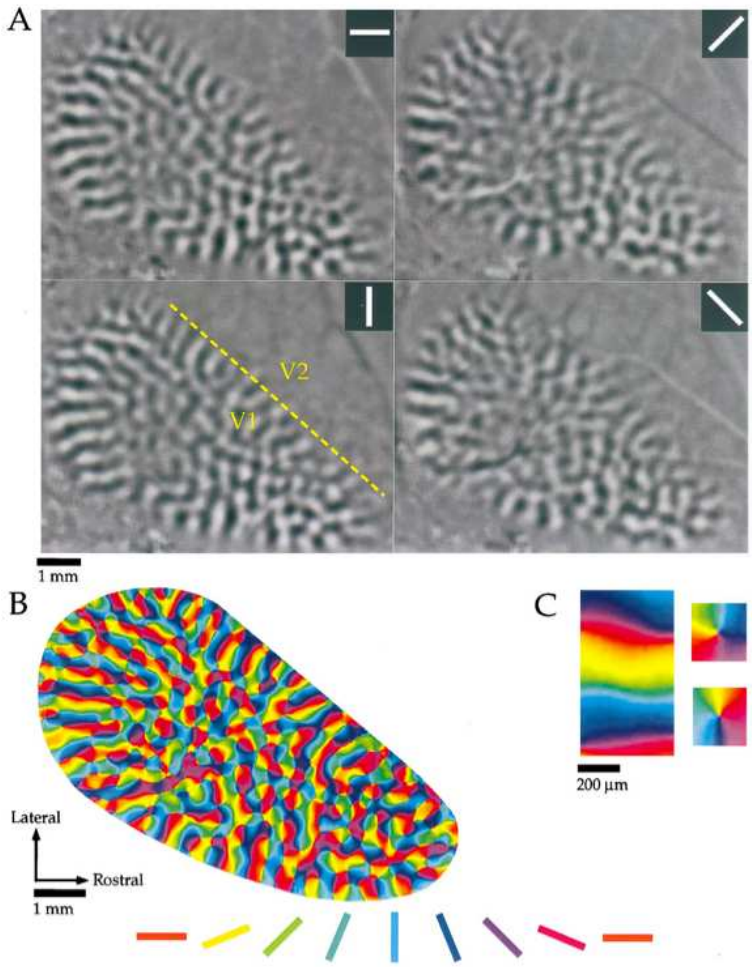

Figure 13: *Optical imaging of intrinsic signals in tree shrew visual cortex. A, Difference images obtained for four stimulus angles. Dark signal indicates areas that were active during presentation of the stimulus. B, Orientation preference map. Orientation preference of each location is color-coded according to the key shown below the map. C, Portions of the orientation preference map shown in B have been enlarged to demonstrate that the orientation preference maps contained both linear zones (left), and pinwheel arrangements (right) that are functional discontinuities (From [6]).*

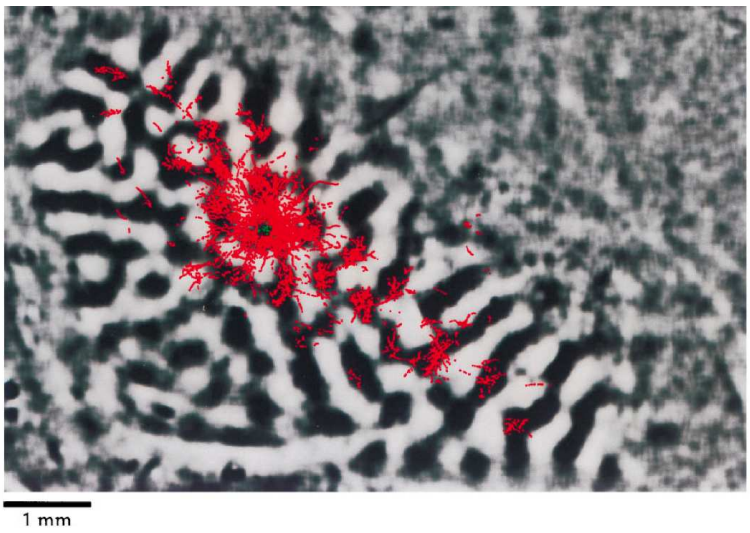

Figure 14: *Reconstruction of axonal boutons distibution (red) from a pool of biocytin-injected pyramidal neurons in layer II/III of the tree shrew visual cortex (green central patch). Strongly marked black and white stripes indicate V1 (black stripes are active areas for a* 90° *stimulus). A central patch of radius* $\sim 500\mu m$ *is observed, surrounded by smaller patches extending over several millimeters (From [6]).*

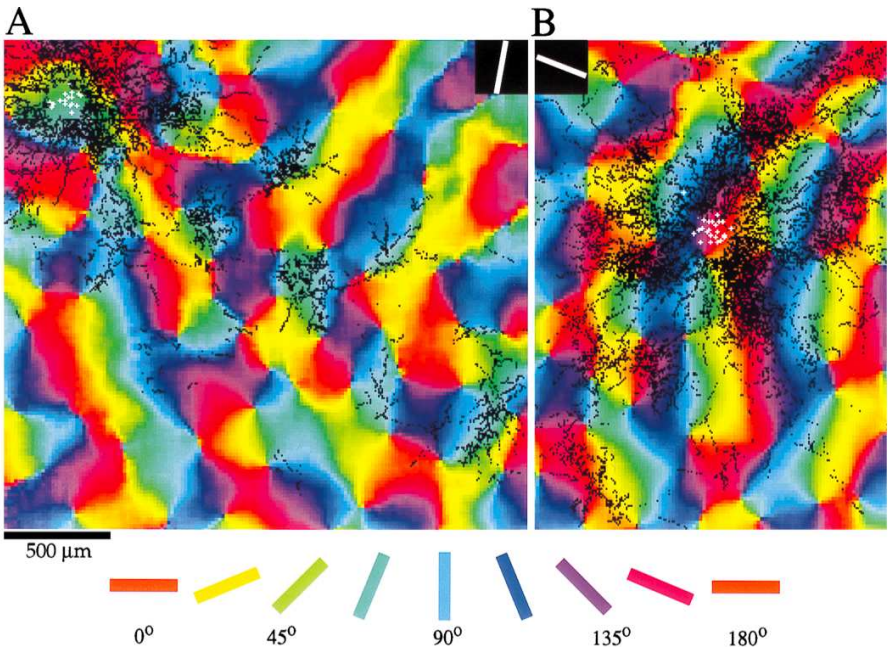

Figure 15: *Reconstruction of axonal boutons distibution (black) from a pool of biocytin-injected pyramidal neurons (white crosses) in layer II/III of the tree shrew visual cortex. A central patch of radius $\sim 500\mu m$ is observed, that show no orientation selectivity. Surrounding smaller patches more acutely match areas with similar orientation preference to the preferred orientation of the injection site. The white bar at the corner of each image indicates the preferred orientation of the injected site (From [6]).*

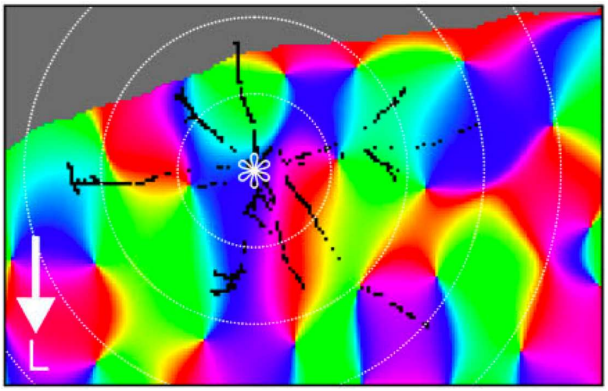

Figure 16: *Projections originating from a single layer III PC. They do not show particularly patchy nor selective characteristics (the white arrow shows the lateral direction) (From [8]).*

So, inhibitory horizontal projections would mainly have two functional roles: distally supressing non-preferred responses, and proximally helping to sharpen orientation and direction tunings because of their looser selectivity compared to excitatory projections.

4.2 Barrel cortex of the rat

The barrel cortex of the rat has a striking columnar organization in layer IV (see figure 18). This layer can be divided into two main regions: the barrels, that somatotopically correspond to whiskers, and the septa, made of the neurons lying between the barrels. Evidence has been shown that barrel- and septum-related pathways are partially segregated. Barrels and septa receive sensory input from different subcortical pathways, and in layer IV, septum cells preferentially innervate other septum cells while barrel cells mostly innervate neurons in the same barrel. This segregation extends to layer II/III because of the focused vertical projections from layer IV spiny cells [7, 17]. We now focus on the connectivity among barrel-related columns defined by the width of barrels in layer IV and spanning the whole depth of the cortex.
Layer IV neurons are basically limited to processing information that originates from the associated whisker and form the predominant source of excitatory inputs to layer II/III, that occur on the basal dendrites of PCs in the same column. On the contrary, layer II/III exhibits both intra- and trans-columnar interactions. So, it appears that this circuitry ensures the segregation of specific tactile stimuli (in layer IV) as well as the transfer of information to neighbouring columns (in layer II/III).
Projections from layer II/III are spatially biased. In this layer, the activity of a single barrel can spread laterally in an oval pattern, preferentially along the rows of the barrel field (corresponding to horizontal rows of whiskers on the rat's muzzle), as anatomically suggested

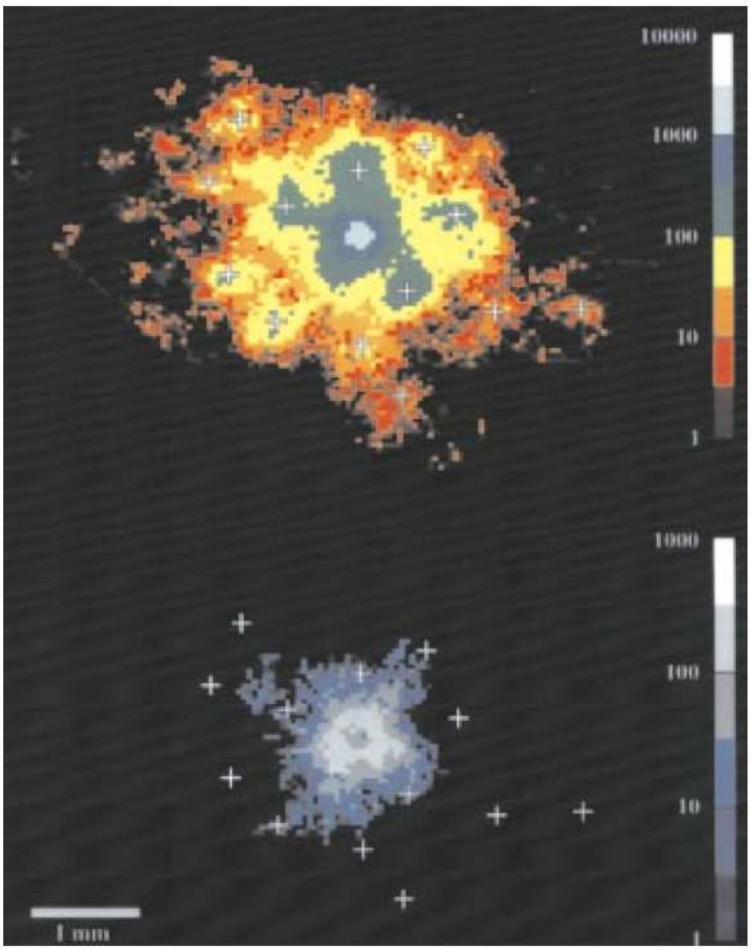

Figure 17: *Comparative distributions of bouton density for pyramidal (up) and basket cells (down). PCs axonal projections form long-range clusters (white crosses) while basket cells ones do not and are less widely spread (From [20]).*

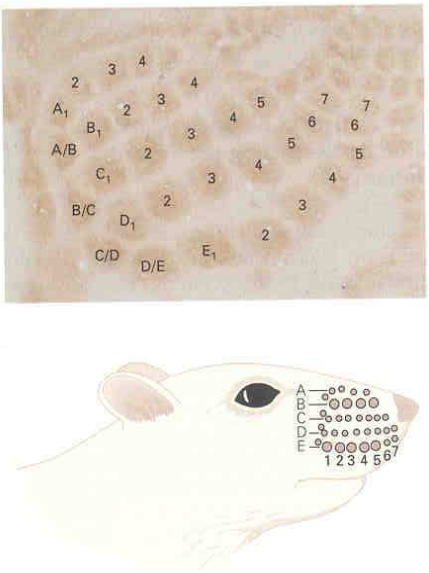

Figure 18: *Layer IV of rat's sensory cortex (stained for serotonin). Every whisker of the rat corresponds to a well defined area of the cortex mostly responsible for processing information from it. These processing units have the same distribution as whiskers on the muzzle. (From [16]).*

by the bias of elongation in the direction of barrel rows observed in apical dendrites and axonal arborizations of layer II/III PCs (see figure 19 and 20). This elongation is also observed in the dendritic trees of deep layers PCs.

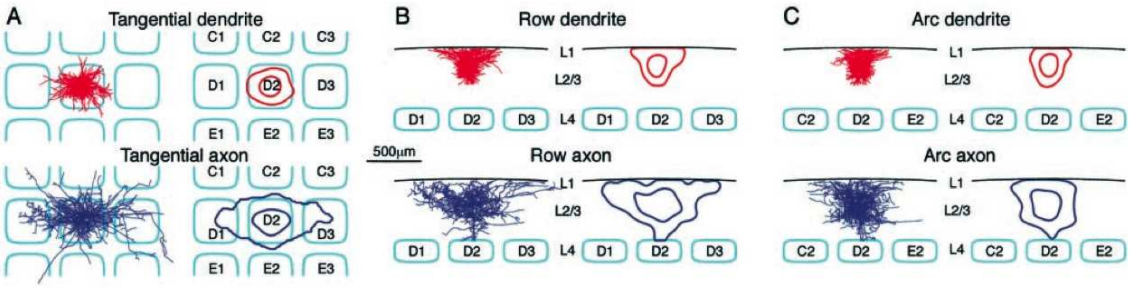

Figure 19: *A. Coronal view of rat barrel cortex (barrels in layer IV are delineated by light blue lines, showing three rows, C, D and E, and three arcs, 1, 2 and 3) showing the preferred elongation of axonal and dendritic trees of layer II/III PCs in the direction of rows. B-C. Corresponding side views (From [23]).*

5 Simulations

5.1 Visual cortex

5.1.1 The line-motion illusion

The line-motion illusion illustrates a well-known Gestalt principle: non-moving stimuli can induce illusory motion perception. A movie displays a static square for a short period of time, followed by a very short period with no stimulus, and then displays a static bar (rectangle). So the movie is a simple square-blank-bar sequence of static stimuli (see figure 21-a). The visual impression is different: it feels like the square is growing into the bar (see figure 21-b). Recent experimental findings report that a correlate of the line-motion illusion has been observed, by VSDOI techniques, in the visual cortex of anaesthetized cats [15].
The experimental paradigm is the following. Cats have been shown several stimuli while their cortical activity was simultaneously monitored by VSDOI and extracellular recordings: a static square stimulus, corresponding to the line-motion paradigm where the part displaying the bar has been truncated (see figure 21-c), a static bar stimulus, corresponding to the line-motion paradigm where the part displaying the square has been truncated (see figure 21-d), a moving square stimulus (see figure 21-e) and the line-motion paradigm (see figure 21-f). Results are shown in figure 21. In the line-motion paradigm, the optical pattern induced by the square (compare to figure 21-c) grows into the optical pattern induced by the bar

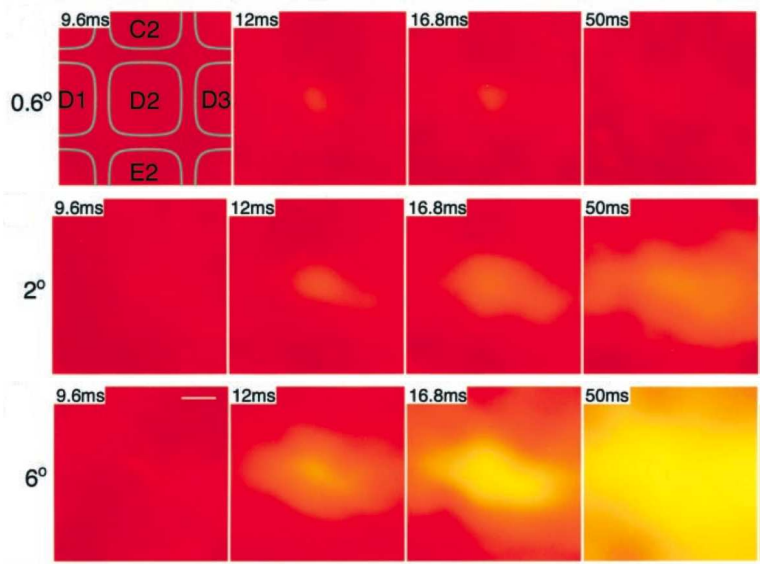

Figure 20: *Response sequences in the rat barrel cortex observed by optical imaging. A single whisker of the animal is stimulated with an increasing angle and speed (top to bottom). In the upper left image, a map of the barrels in layer IV is superimposed. A weak stimulation of the whisker provoke an activation in the column of barrel D2 (upper sequence). Stronger stimulation results in graded horizontal spread of activity (middle and bottom sequences) (From [23]).*

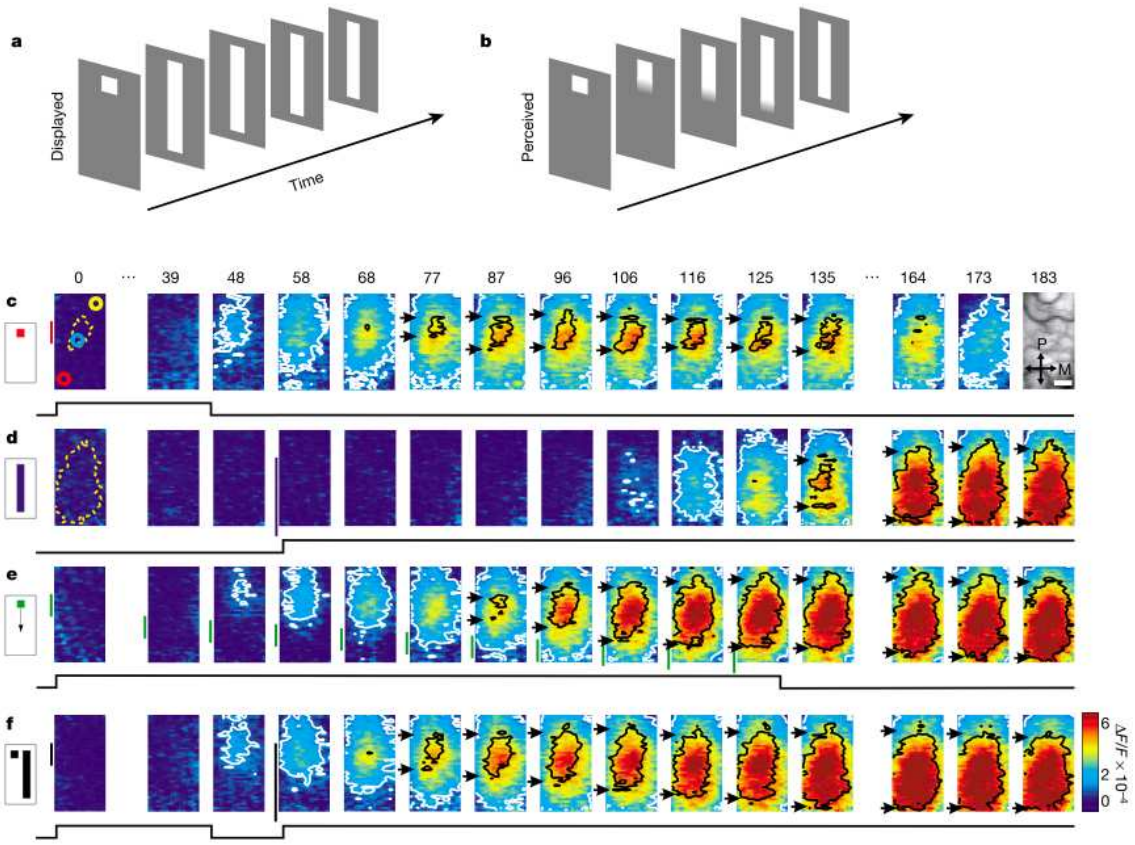

Figure 21: *Line-motion illusion and its cortical correlates. (a) Stimulus of the line-motion paradigm. (b) Corresponding illusory motion percept. (c-f) Optical signals recorded for different stimuli (c: flashed small square, d: flashed bar, e: moving small square, f: line-motion paradigm). Stimuli are indicated on the left, their duration at the bottom of optical sequences and time after stimulus onset (in milliseconds), at the top of the panels. Yellow dotted contours approximate retinotopic representation of the stimuli; colored circles indicate extracellular recording sites; white contours delimit low-amplitude activity and black contours, high-amplitude activity. Color scale indicates averaged fractional changes (i.e. normalized with ongoing activity without stimulation) in fluorescence intensity. The cortical area imaged is shown in the upper right panel. Scale bar: 1 mm, P: posterior, M: medial. (From [15]).*

(compare to figure 21-d). The propagation of the neuronal activity has been confirmed by the simultaneous extracellular recordings, showing that the propagation is not due to a property of optical imaging signals. Moreover, the optical signal obtained in the line-motion paradigm is similar to the signal obtained with a moving stimulus (compare e and f). These results suggest that the line-motion illusion has a correlate in terms of neuronal activity in V1.

5.1.2 Parametrization

We try to reproduce the optical signals presented in figure 21.
To that purpose we simulate an activity-based neural field model including axonal propagation delays of the form

$$\dot{\mathbf{A}}(\mathbf{r},t) = -\mathbf{L}\mathbf{A}(\mathbf{r},t) + \mathbf{S}\left(\int_{\Omega} \mathbf{W}(\mathbf{r}-\mathbf{r}')\mathbf{A}(\mathbf{r}', t-\|\mathbf{r}-\mathbf{r}'\|/c))\, d\mathbf{r}' + \mathbf{I}_{\text{ext}}(\mathbf{r},t)\right) \qquad (6)$$

with the following parameters:

- *Populations.* We use the populations proposed in [13] ($N = 6$): three layers (II/III, IV and V) with excitatory and inhibitory neurons in each.
- *Field* Ω. Square domain with a side length of $1cm$, discretized in 100×100 units. No orientation preference consideration is made.
- *Time.* We integrate the equation over 80 time steps of $2.5ms$, corresponding to a total duration of $200ms$.
- *Axonal delays c.* We add delays to the neural field equation, due to finite axonal propagation speed. We have chosen $c = 10cm/s$, in agreement with the actual propagation speed in the visual cortex of the cat.
- *Synaptic time constants* $\mathbf{L}$. Two synaptic time constants: $\tau_e = 100ms$, used for all excitatory neurons, and $\tau_i = 200ms$ for all inhibitory neurons. Inhibitory postsynaptic potentials are indeed slower than excitatory ones. The time constant of real EPSPs is around $10ms$ and the one of $GABA_A$-mediated IPSPs around $100ms$ [25]. However we choose slower synaptic characteristic times to ensure the stability of the numeric scheme we have used for simulations.
- *Wave-to-pulse transforms* $\mathbf{S}$. Two transforms: S_e (for all types of excitatory cells) and S_i (for all types of inhibitory cells), of the form

  $$S_x(v) = \frac{\overline{\nu}_x}{1 + \exp(r_x\,(v_0^x - v))}, \quad x \in \{e, i\},$$

  with maximal firing rates $\overline{\nu}_e = \overline{\nu}_i = 7.5Hz$, gains $r_e = r_i = 0.5mV^{-1}$, and excitability thresholds $v_0^e = 3mV$ and $v_0^i = 6mV$. Inhibitory neurons are indeed less excitable than excitatory ones. However, their maximal firing rates are usually higher than the ones of excitatory cells, which has not been taken into account here.

- *Connectivity* $\mathbf{W}$. We choose translation-invariant connectivity kernels $W_{ij}(\mathbf{r}-\mathbf{r}')$, defined on $\widehat{\Omega}=[-1,1]^2$, and define *global weights* as

$$\overline{W}_{ij}=\int_{\widehat{\Omega}} W_{ij}(\mathbf{r})\,d\mathbf{r}.$$

Vertical connectivity is defined by the global weights and horizontal connectivity, by normalized connectivity kernels

$$\widehat{W}_{ij}(\mathbf{r})=W_{ij}(\mathbf{r})/\overline{W}_{ij},\quad \mathbf{r}\in\widehat{\Omega},$$

so that

$$\int_{\widehat{\Omega}} \widehat{W}_{ij}(\mathbf{r})\,d\mathbf{r}=1.$$

The global weights are set in agreement with the six population model proposed in [13]. They are scaled by k_{ij}, w_{ij} and N_j. k_{ij} and w_{ij}, the average synaptic gains and connection probabilities, are given in [13]. As concerns N_j, we consider columns with 160 excitatory neurons and 40 inhibitory neurons (in agreement with proportions reported for mammals cortex), and distribute them equally among layers (this choice is supported by recent experimental findings [4]). A color-coded version of the vertical connectivity matrix $\overline{\mathbf{W}}$ is given in figure 22.

The form of the $\widehat{W}_{ij}$s mostly depends on the horizontal spread of the axonal arbors of neurons of type j[6], and on whether they make patches or not. Local projections from inhibitory neurons are modeled by a circularly symmetric Gaussian distribution with a standard deviation (SD) of $0.7mm$. Projections from layer IV excitatory cells, among which spiny stellate excitatory interneurons are largely represented, are also modeled by a unique local patch, but with a larger extent ($SD=0.8mm$) to account for longer range projections made by layer IV PCs (see figure 23).

Finally, projections from PCs in layers II/III and V (see figure 24) are modeled by a central local patch $\widehat{W}^{\mathrm{c}}_{ij}$ ($SD=0.4mm$) surrounded by six satellite patches of the same extent, forming the component $\widehat{W}^{\mathrm{sat}}_{ij}$. Hence

$$\widehat{W}_{ij}=\widehat{W}^{\mathrm{c}}_{ij}+\widehat{W}^{\mathrm{sat}}_{ij}.$$

The distance between the center of the central patch and the centers of the satellite patches is set to $1.25mm$. Actually, most projections corresponding to satellite patches do not stand for local projections in the sense of local connectivity studies, because they outreach the extent of a cortical column. Hence the global weight obtained from local connectivity studies for PCs projections should be mainly attributed to the central patch. So as j corresponds to a PC population, we choose

$$\int_{\widehat{\Omega}} \widehat{W}^{\mathrm{c}}_{ij}(\mathbf{r})\,d\mathbf{r}=1\quad\text{and}\quad\int_{\widehat{\Omega}} \widehat{W}^{\mathrm{sat}}_{ij}(\mathbf{r})\,d\mathbf{r}=1,$$

[6] Here we neglect the extent of the dendritic trees of neurons of type i.

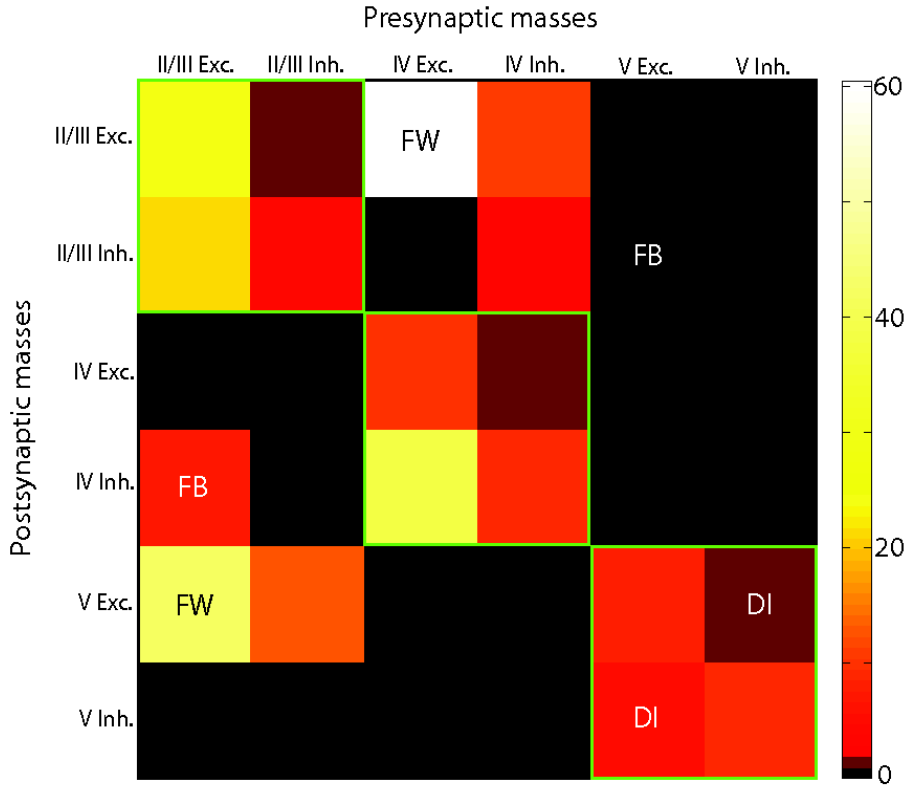

Figure 22: *Color-coded vertical connectivity matrix (connection strength $\overline{W}_{ij}$ is expressed in mV). Green squares indicate intralaminar connections. Well-identified pathways are also mentioned: excitatory forward (FW) and feedback (FB) interlaminar pathways, as well as connections involved in disynaptic inhibition (DI). The feedback arising from layer V PCs and connections corresponding to disynaptic inhibition are probably underestimated in this model, due to a lack of available connectivity data.*

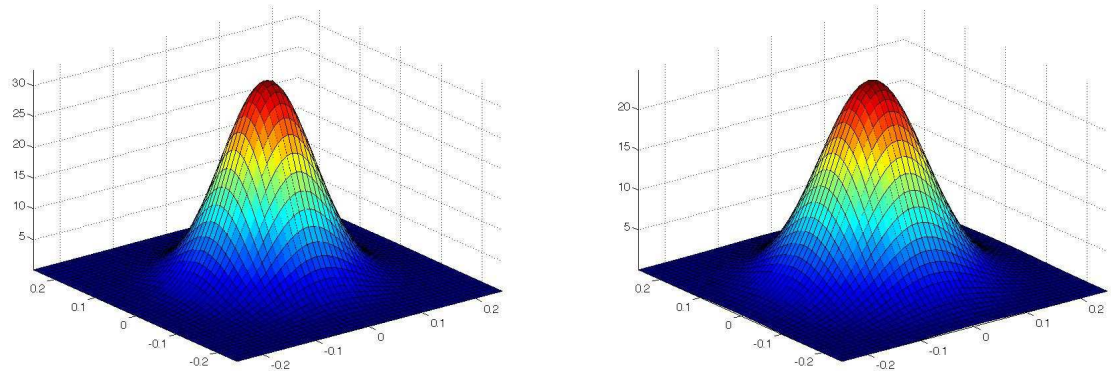

Figure 23: . *Form of the non-patchy projections made by inhibitory neurons (left) and layer IV spiny cells (right), represented on a subdomain of* $\widehat{\Omega}$ *(abscissas are expressed in cm).*

so that

$$\int_{\widehat{\Omega}} \widehat{W}_{ij}(\mathbf{r})\, d\mathbf{r} = 2.$$

This choice is in good agreement with biological data, since in [8], the authors report a number of axonal boutons in the central patch equivalent to the number of boutons in all satellite patches.

- *Input* $\mathbf{I}_{\text{ext}}$. The input terms correspond to the various paradigms we want to simulate, modified by a spatiotemporal regularization accounting for the effect of the retino-cortical pathway. So to obtain $\mathbf{I}_{\text{ext}}$ the stimulus is first convoluted with a Gaussian spatial kernel ($SD = 0.35mm$), modeling the horizontal spread of afferent thalamic fibers in layer IV.
  Then a temporal kernel $T(t)$ of the form

$$T(t) = \begin{cases} e^{-t/\tau}/\tau & t \geq 0 \\ 0 & t < 0 \end{cases}, \quad \tau = 35ms$$

moderates the signal, accounting for both retino-thalamic persistence and adaptation to the visual input [1]. This kernel acts as follows. Any newly activated pixel in the stimulus sequence will follow the time course of T, regardless of whether the pixels continues to be activated or not. Hence transiently activated pixels will persist at the level of the thalamo-cortical input and persistently activated pixels will undergo adaptation. This retino-thalamic temporal regularization, as suggested in [24], is crucial in the moving square case.

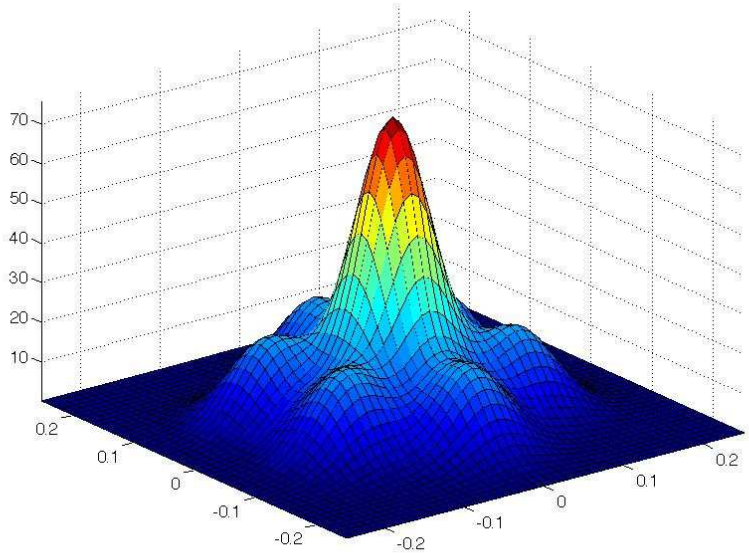

Figure 24: *Form of the patchy projections made by PCs from layers II/III and V, represented on a subdomain of* $\widehat{\Omega}$ *(abscissas are expressed in cm).*

A delay of $40ms$ for visual input arrival to the cortex is modeled by giving $\mathbf{I}_{\text{ext}}$ an initial $40ms$ of blank, followed by the stimulus. In stimuli, the background is set to zero and light patterns (square or bar) to one. Stimuli project exclusively on layer IV, with an equal repartition between excitatory and inhibitory neurons. The stimuli and the corresponding inputs to the cortex are shown in figure 25.

- *Optical signal.* Since dendritic trees lying in layer I-III are the main contributors to the optical signal, we choose to neglect contributions from other layers ($n_{\text{I-III}} = 1$ and other n_ls set to zero). Layer I-III mostly contains dendrites belonging to all types of neurons from layers II/III and PCs from layer V (see figure 11). Hence, up to a multiplicative constant, the optical signal is

$$\sum_{j=1}^{N} \int_{\Omega} \left(\sum_{i=1}^{3} N_i \, s_i^{\text{I-III}} \, \alpha_{ij}^{\text{I-III}} \, W_{1j}(\mathbf{r}, \mathbf{r}') \right) A_j(\mathbf{r}', t) \, d\mathbf{r}',$$

where $i = 1$, 2 and 3 are, respectively, the indices of layer II/III PCs, layer V PCs and superficial layers interneurons. Now, for clarity, we choose to normalize the coefficients $N_i \, s_i^{\text{I-III}} \, \alpha_{ij}^{\text{I-III}}$ by $N_1 \, s_1^{\text{I-III}} \, \alpha_{1j}^{\text{I-III}}$. We consider that $s_1^{\text{I-III}} \approx s_2^{\text{I-III}}$ and that $N_1 = N_2$ (as assumed in the model). PCs from layer II/III receive all their inputs at the level of layers I-III ($\alpha_{1j}^{\text{I-III}} = 1$) and we assume that PCs from layer V receive half of all their inputs on their superficial dendrites ($\alpha_{2j}^{\text{I-III}} = 1/2$). Hence the normalized coefficient for layer II/III PCs is 1 and the one for layer V PCs, 1/2. The diameter and total length of interneurons dendrites are inferior to the ones of PCs [4, 5]. Hence the normalized coefficient of inhibitory cells is less than N_2/N_1. We choose it to be 1/10. So we end up with

$$OI(\mathbf{r}, t) \approx \sum_{j=1}^{N} \int_{\Omega} \left(W_{1j}(\mathbf{r}, \mathbf{r}') + \frac{1}{2} W_{2j}(\mathbf{r}, \mathbf{r}') + \frac{1}{10} W_{3j}(\mathbf{r}, \mathbf{r}') \right) A_j(\mathbf{r}', t) \, d\mathbf{r}'.$$

5.1.3 Results

Figure 26 shows the optical imaging sequences obtained from the simulation of the neural field with different stimuli (the observation window is a rectangle of side lengths $3mm$ and $5mm$). As in [15], we have normalized the results with blanks (i.e. simulations of a field receiving no input). The intensity of the signal is then expressed as a percentage.
We have been able to reproduce the main features of the optical signals from figure 21.

- The optical signals corresponding to the moving square and the line-motion paradigm have similar temporal sequences.
- In both cases, the activity pattern induced by a square stimulus progressively grows into the pattern induced by a bar stimulus[7].

[7] In the moving square case, a bleeding input has been necessary to keep a homogeneous level of signal on the whole extent of the bar pattern.

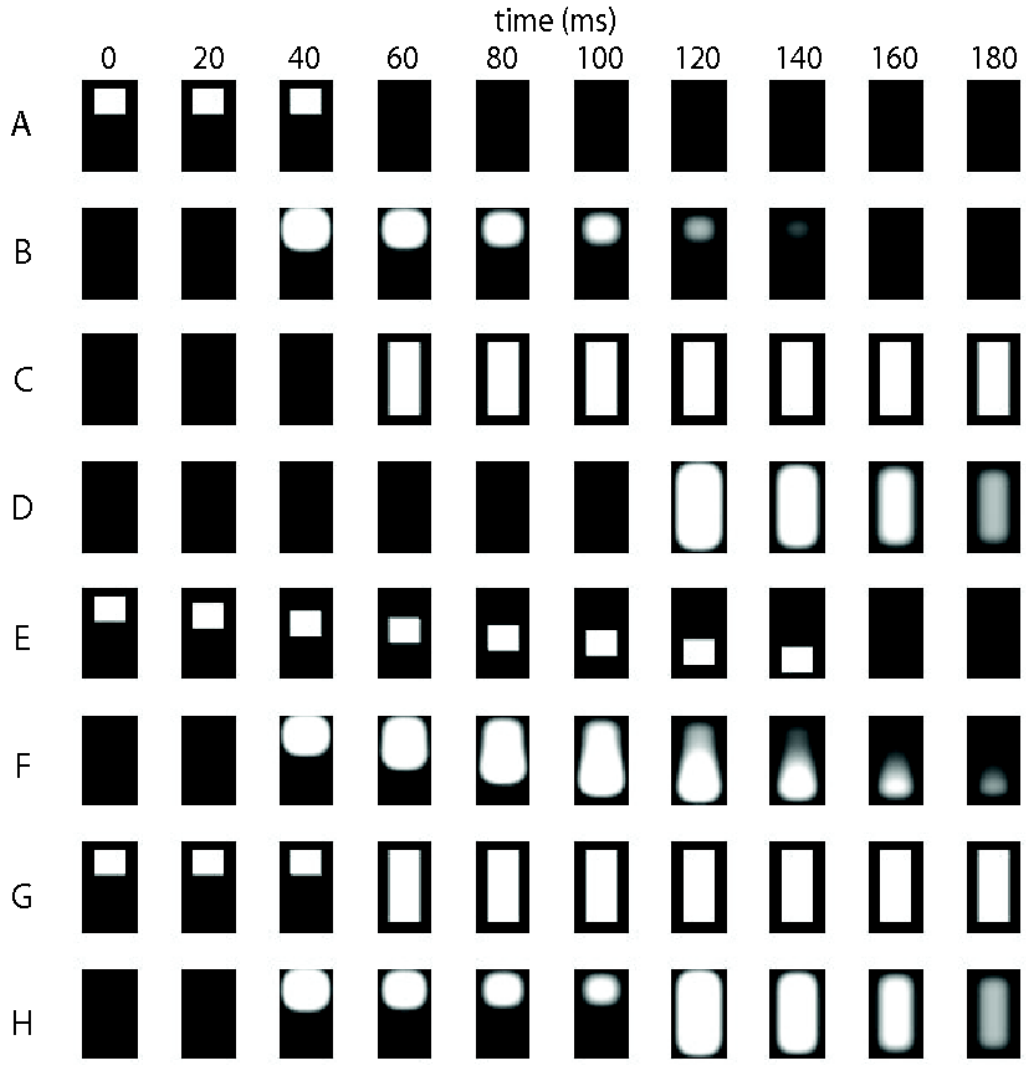

Figure 25: *Stimuli and corresponding cortical inputs obtained after spatio-temporal regularization and time translation. They are presented on a subdomain of* Ω *(*$[0.35, 0.65] \times [0.25, 0.75]$*). A-B: square, C-D: bar, E-F: moving square, G-H: line-motion paradigm.*

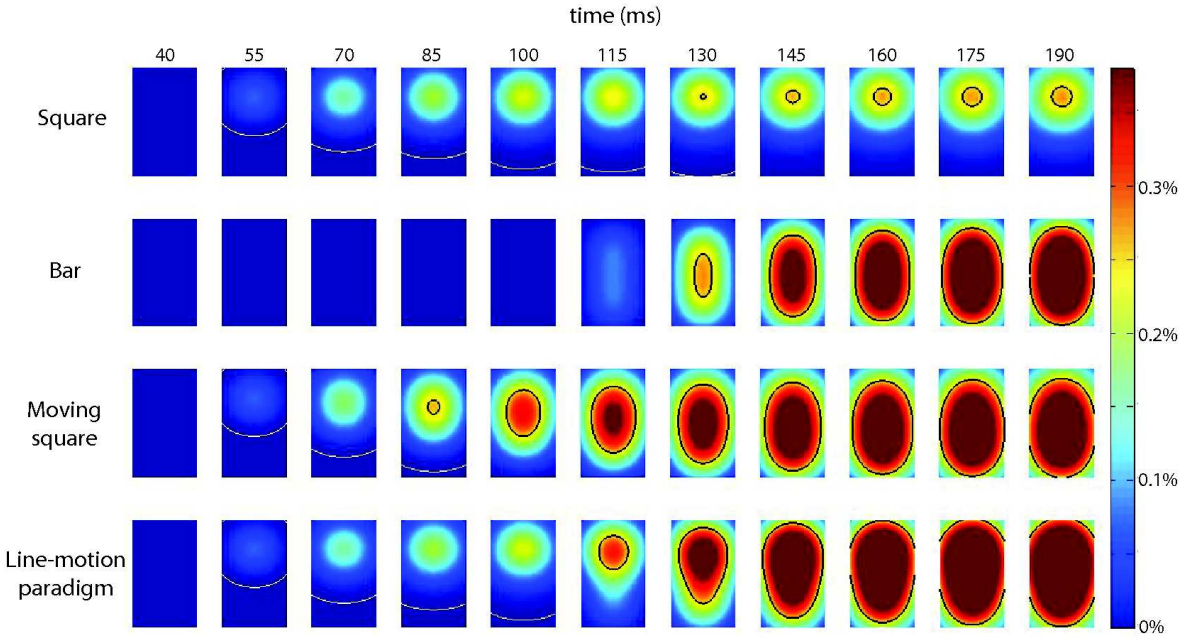

Figure 26: *Simulated optical sequences obtained for different stimuli and reproducing the main features of experimental results (see text). White lines delineate low-level activity ($OI < 0.002\%$) and black lines, high-level activity ($OI > 0.25\%$).*

- In the case of the line-motion paradigm, the spatial propagation of activity is obtained with a static input.
- The cortical input corresponding to a *growing square* stimulus (featuring a square growing into a bar) is exactly the same as the one corresponding to the moving square, as an effect of the spatio-temporal regularization. Hence, the optical activity induced by this stimulus is identical to the one obtained for the moving square. This is in good agreement with the results of [15], where the authors observe a very good match between the optical signals recorded for the growing square, the moving square and the line-motion paradigm.
- High activity is maintained over time, even in the absence of a strong input.

5.2 Barrel cortex

Now we try to reproduce the spread of activity in the barrels of the rat's sensory cortex as one whisker is stimulated with different intensities. The results of this experimental paradigm are shown in figure 20 [23]. A weak stimulation of a single whisker induces a low, transient activation of the corresponding barrel. As the stimulation strength is increased, cortical activity propagates to the row of the excited barrel. As the stimulation gets strong enough, the activity propagates to the whole barrel field.

5.2.1 Parametrization

For this simulation we use the same neuronal populations, neural field equation, axonal propagation speed, synaptic time constants, wave-to-pulse transforms and optical signal as for the visual cortex case. Changes in parametrization are given below.

- *Field* Ω. Square domain with a side length of $1mm$, discretized in 100×100 units. Barrels and septa regions are segregated (see figure 27).
- *Time*. We integrate the equation over 20 time steps of $2.5ms$, corresponding to a total duration of $50ms$.
- *Connectivity* $\mathbf{W}$. Vertical connectivity is the same as in the visual cortex case. Horizontal connectivity depends on barrels and septa and on the involved types of neurons. We consider two two-dimensional Gaussian distributions G_1 and G_2. G_1 is isotropic and has a small standard deviation $SD = 80\mu m$. G_2 is elongated in the direction of barrel rows and is defined by two standard deviations corresponding to its principal axes: $SD = 80\mu m$ and $SD' = 400\mu m$ (see figure 28).

  If the presynaptic neurons belong to a column of the septum, $\widehat{W}_{ij} = G_1$ for all couples (i, j). Hence, septum masses mostly innervate other septum masses in their immediate neighborhood. If the presynaptic neurons belong to a barrel and are not layer II/III PCs, we also have $\widehat{W}_{ij} = G_1$. Hence they mostly target neurons from the same barrel.

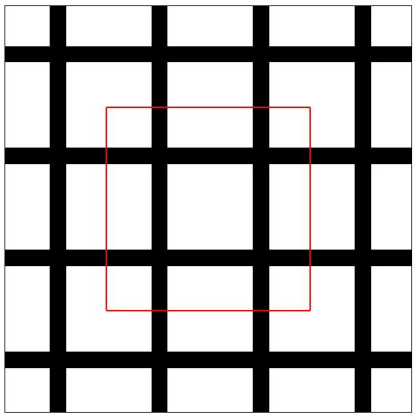

Figure 27: *The field Ω is separated into two regions: barrels (in white) and septa (in black). The red contour delineates the observation window on which we will display the results of the simulations.*

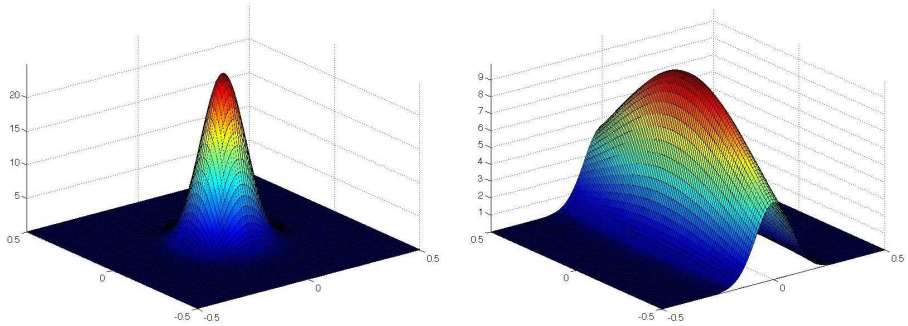

Figure 28: *Gaussian connectivity kernels. G_1 (left) is isotropic and has a standard deviation $SD = 80\mu m$. G_2 (right) is elongated in the direction of barrel rows ($SD' = 400\mu m$).*

When presynaptic neurons are layer II/III PCs belonging to a barrel, they can reach more distant postsynaptic targets: neurons in the same layer, via their elongated axonal projections, and layer V PCs, whose basal dendritic trees are also elongated. So $\widehat{W}_{ij} = G_2$ if i is the index of layer II/III PCs, layer II/III inhibitory cells, or layer V PCs. Otherwise, $\widehat{W}_{ij} = G_1$.

- *Input* $\mathbf{I}_{\text{ext}}$. The input is a brief ($5ms$), spatially isotropic stimulation confined to the central barrel of the observation window, arriving to the cortex at $t = 10ms$. It is focused on layer IV, targeting equally excitatory and inhibitory cells. Three such spatially focused inputs are used in the simulations shown below, with different intensities and widths. They model the single whisker deflections of various angle and acceleration used in [23] (see figure 29).

5.2.2 Results

The results of the simulations are given in figure 30.
The simulations reproduce the main features of the experimental results. For a weak stimulation, we observe the low, transient and isotropic activation of a single barrel. For stronger stimulations, we first observe isotropic activity patterns ($t = 17.5ms$) which are progressively elongated in the direction of the barrel row ($t = 20ms$). If the stimulation is strong and wide enough, the activity propagates to other rows, leading to a rapid extension of activity to the whole field (strong stimulus). For milder stimulations, activity fails to propagate to other rows and remains confined in the row of the stimulated whisker (moderate stimulus).

6 Discussion

Starting from biophysical neural field models of sensory cortices and using the previously developed direct problem formula, we have been able to reproduce realistic optical imaging sequences from various experimental settings.

The simulations that we have presented in the last section mainly involved two phenomena: propagation and persistence of cortical activity. Propagation of the signal is principally a matter of horizontal connectivity: wide horizontal connectivity kernels guarantee a good horizontal propagation. A bias in the direction of propagation can be induced by a bias in the form of the kernels (case of the rat barrel cortex) or by a moving thalamic stimulation (case of the moving square). When the field is fed by static stimuli, as in the line-motion paradigm, propagation is a nonlinear effect induced by simultaneous stimulations of the field by horizontal projections and thalamic inputs: a thalamic stimulation in the neighborhood of an active domain of the field will lead to the propagation of the activity in the direction of the input. The neural field model is naturally persistent, even in absence of thalamic stimulation, thanks to the finite speed of axonal and dendritic processes. However, a stronger persistence is needed in the moving square case. The determining parameter for this phenomenon is the latency of the retino-thalamic pathway τ. τ has been set long enough for

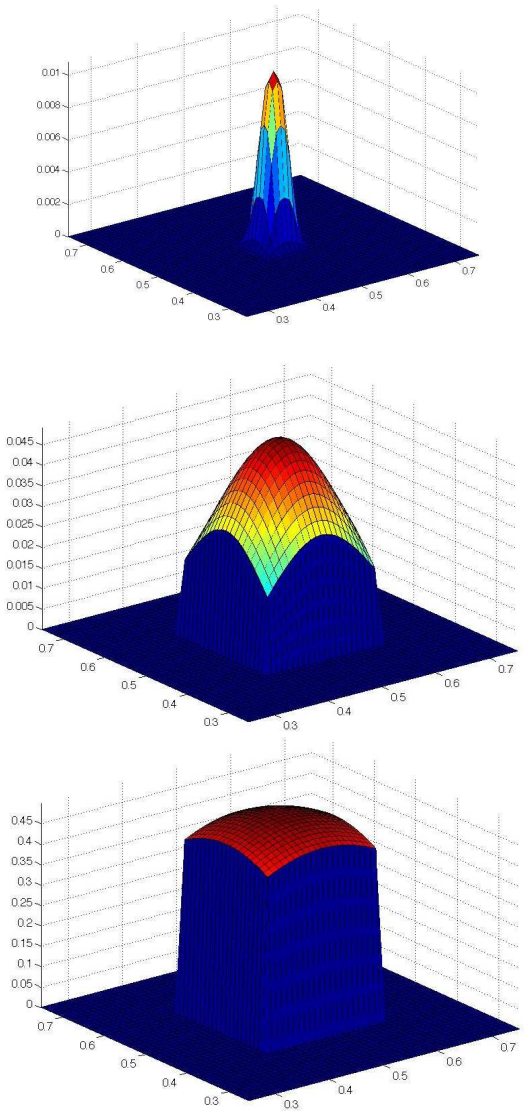

Figure 29: *Form of the single whisker stimulations used in the simulations, represented on the observation window domain. All of these stimuli are restricted to the excited barrel and are isotropic. On the upper left panel, a narrow, low intensity stimulus corresponds to a weak input. On the upper right panel, a stronger and wider stimulus accounts for moderate stimulation. The input corresponding to a strong stimulation is represented on the lower panel and shows larger horizontal extent and intensity.*

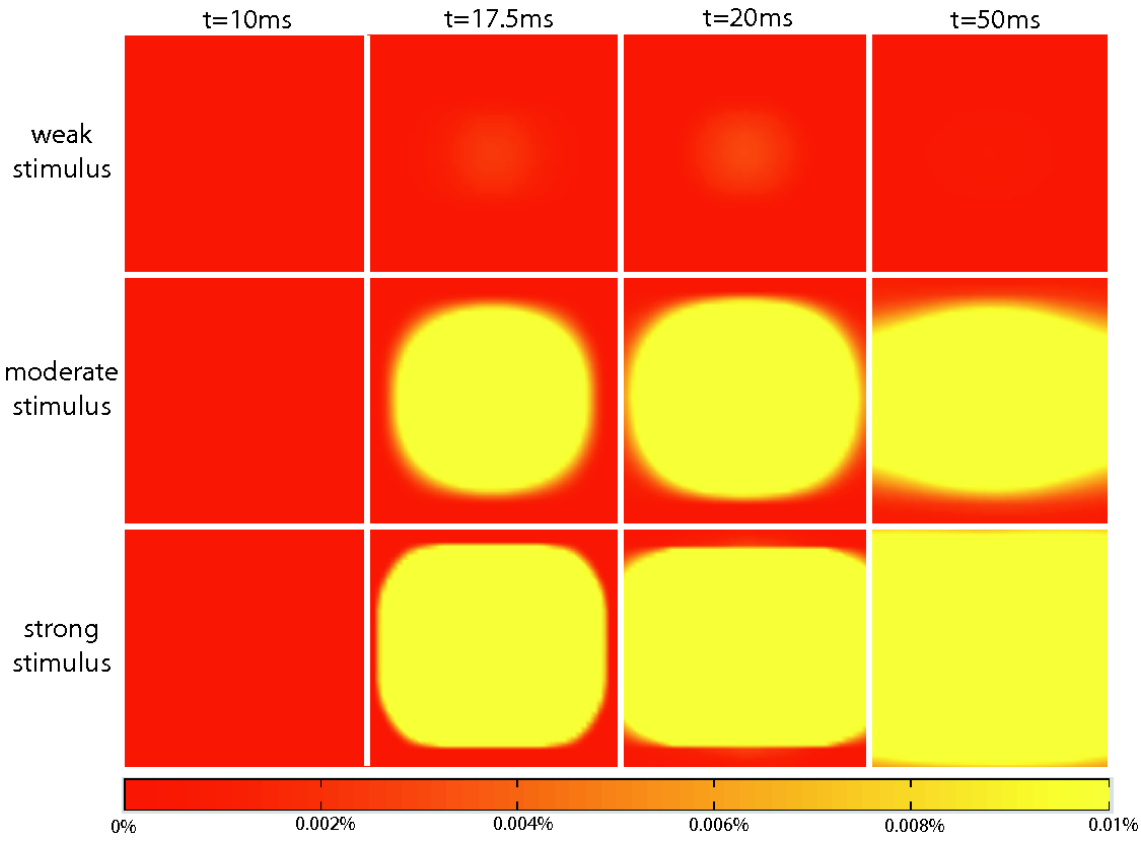

Figure 30: *Simulated optical sequences obtained for different intensities of single whisker stimulation. They reproduce the main features of the experimental results presented in [23]. A weak stimulation induces a low and transient activation of a single barrel (upper panel). As the stimulation intensity increases, the activity propagates to a whole barrel row (middle panel). For strong stimulations, the activation spans over the whole barrel field (lower panel).*

the moving square activation to persist on the whole length of the bar activity pattern, and short enough to avoid a strong, sustained thalamic stimulation leading to inhomogeneities in the activation patterns. For example, in the line-motion paradigm, a sustained, strong excitation during the square part of the stimulus will make the subsequent activation due to the rest of the bar relatively small, while we want an homogeneous activation of the pattern induced by the bar, as a natural effect of adaptation.

Biophysical models are probably not necessary to reproduce the most basic features of the optical signals and it would be interesting to develop minimal models for which a rigorous mathematical explanation of the observed phenomena would be tractable. For example, connectivity patches are not needed in the neural field model of the visual cortex for the model to reproduce experimentally observed phenomena. The crown of satellite patches surrounding the central patch in excitatory kernels could be replaced by an isotropic annulus. Although, the model should not be oversimplified. Following the same example, if we replace the patchy connectivity kernels by simple Gaussians, we will observe undesirably narrow or broad spreads of activity. This is avoided in our simulations thanks to the predominance of inhibition between the central excitatory patch and the satellite patches, preventing localized inputs to provoke too broad activations and allowing extended inputs to induce extended activations, via long-range excitation (see figure 31).

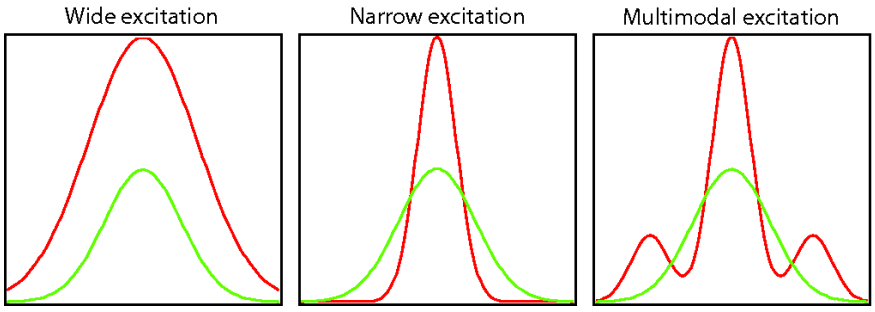

Figure 31: *Unimodal vs multimodal excitation. Excitatory (resp. inhibitory) kernels are represented in red (resp. green). Unimodal excitatory connectivity kernels can have two effects on the horizontal propagation of activity. A wide unimodal excitatory kernel that dominates inhibition (left) can induce too broad activations of the field. On the contrary, a narrow unimodal excitatory kernel (center) does not allow broad activations. Finally, a multimodal kernel moderates the spread of localized stimulations thanks to middle-range inhibition, and allows widespread activations thanks to long-range excitation.*

So, although some aspects of the model could be simplified, the very general framework of neural fields allowed us to integrate biologically plausible parameters and to account for the organizing principles of different cortices within a relatively small set of parameters.

References

[1] LF Abbott and W.G. Regehr. Synaptic computation. *Nature*, 431:796–803, 2004.

[2] A. Ajima and S. Tanaka. Spatial Patterns of Excitation and Inhibition Evoked by Lateral Connectivity in Layer 2/3 of Rat Barrel Cortex. *Cerebral Cortex*, 16(8):1202, 2006.

[3] P Bannister. Inter- and intra-laminar connections of pyramidal cells in the neocortex. *Neuroscience Research*, 53(2):95–103, 2005.

[4] T. Binzegger, R.J. Douglas, and K.A.C. Martin. Stereotypical Bouton Clustering of Individual Neurons in Cat Primary Visual Cortex. *Journal of Neuroscience*, 27(45):12242, 2007.

[5] Tom Binzegger, R.J. Douglas, and K.A.C. Martin. A quantitative map of the circuit of cat primary visual cortex. *The Journal of Neuroscience*, 24(39):8441–8453, September 2004.

[6] W.H. Bosking, Y. Zhang, B. Schofield, and D. Fitzpatrick. Orientation selectivity and the arrangement of horizontal connections in tree shrew striate cortex. *The Journal of Neuroscience*, 17(6):2112–2127, 1997.

[7] M. Brecht, A. Roth, and B. Sakmann. Dynamic receptive fields of reconstructed pyramidal cells in layers 3 and 2 of rat somatosensory barrel cortex. *The Journal of Physiology*, 553(1):243–265, 2003.

[8] P. Buzás, K. Kovacs, A.S. Ferecskó, JM Budd, UT Eysel, and Z.F. Kisvárday. Model-based analysis of excitatory lateral connections in the visual cortex. *J Comp Neurol*, 499(6):861–881, 2006.

[9] D. Feldmeyer, J. Lübke, and B. Sakmann. Efficacy and connectivity of intracolumnar pairs of layer 2/3 pyramidal cells in the barrel cortex of juvenile rats. *The Journal of Physiology*, 575(2):583, 2006.

[10] W.J. Freeman. Mass action in the nervous system. *Academic Press, New York*, 1975.

[11] J.P. Gottlieb and A. Keller. Intrinsic circuitry and physiological properties of pyramidal neurons in rat barrel cortex. *Experimental Brain Research*, 115(1):47–60, 1997.

[12] A. Grinvald and R. Hildesheim. VSDI: a new era in functional imaging of cortical dynamics. *Nature Reviews Neuroscience*, 5(11):874–885, 2004.

[13] Stefan Haeusler and Wolfgang Maass. A statistical analysis of information-processing properties of lamina-specific cortical microcircuits models. *Cerebral Cortex*, 17:149–162, jan 2007.

[14] D.H. Hubel and T.N. Wiesel. Functional architecture of macaque monkey. *Proceedings of the Royal Society, London B*, pages 1–59, 1977.

[15] D. Jancke, F. Chavane, S. Naaman, and A. Grinvald. Imaging cortical correlates of illusion in early visual cortex. *Nature*, 428:423–426, 2004.

[16] E.R. Kandel, J.H. Schwartz, and T.M. Jessel. *Principles of Neural Science*. McGraw-Hill, 4th edition, 2000.

[17] U. Kim and F.F. Ebner. Barrels and septa: Separate circuits in rat barrel field cortex. *The Journal of Comparative Neurology*, 408(4):489–505, 1999.

[18] ZF Kisvárday, JM Crook, P. Buzás, and UT Eysel. Combined physiological-anatomical approaches to study lateral inhibition. *J Neurosci Methods*, 103(1):91–106, 2000.

[19] Z.F. Kisvárday, A.S. Ferecskó, K. Kovács, P. Buzás, J.M.L. Budd, and U.T. Eysel. One axon-multiple functions: Specificity of lateral inhibitory connections by large basket cells. *Journal of Neurocytology*, 31(3):255–264, 2002.

[20] ZF Kisvárday, E. Tóth, M. Rausch, and UT Eysel. Orientation-specific relationship between populations of excitatory and inhibitory lateral connections in the visual cortex of the cat. *Cerebral Cortex*, 7:605–618, 1997.

[21] M.T. Lippert, K. Takagaki, W. Xu, X. Huang, and J.Y. Wu. Methods for Voltage-Sensitive Dye Imaging of Rat Cortical Activity With High Signal-to-Noise Ratio. *Journal of Neurophysiology*, 98(1):502, 2007.

[22] J. Lübke, A. Roth, D. Feldmeyer, and B. Sakmann. Morphometric Analysis of the Columnar Innervation Domain of Neurons Connecting Layer 4 and Layer 2/3 of Juvenile Rat Barrel Cortex. *Cerebral Cortex*, 13(10):1051–1063, 2003.

[23] C.C.H. Petersen, A. Grinvald, and B. Sakmann. Spatiotemporal dynamics of sensory responses in layer 2/3 of rat barrel cortex measured in vivo by voltage-sensitive dye imaging combined with whole-cell voltage recordings and neuron reconstructions. *The Journal of Neuroscience*, 23(3):1298–1309, 2003.

[24] A.V. Rangan, D. Cai, and D.W. McLaughlin. Inaugural Article: Modeling the spatiotemporal cortical activity associated with the line-motion illusion in primary visual cortex. *Proc Natl Acad Sci US A*, 102(52):18793–18800, 2005.

[25] P.A. Salin and J. Bullier. Corticocortical connections in the visual system: structure and function. *Psychol. Bull.*, 75:107–154, 1995.

[26] D. Schubert, R. Kötter, and J.F. Staiger. Mapping functional connectivity in barrel-related columns reveals layer-and cell type-specific microcircuits. *Brain Structure and Function*, 212(2):107–119, 2007.

[27] D. Schubert, J.F. Staiger, N. Cho, R. Kötter, K. Zilles, and H.J. Luhmann. Layer-Specific Intracolumnar and Transcolumnar Functional Connectivity of Layer V Pyramidal Cells in Rat Barrel Cortex. *Journal of Neuroscience*, 21(10):3580, 2001.

[28] A. Stepanyants, J.A. Hirsch, L.M. Martinez, Z.F. Kisvárday, A.S. Ferecskó, and D.B. Chklovskii. Local Potential Connectivity in Cat Primary Visual Cortex. *Cerebral Cortex*, 2007.

[29] T.R. Tucker and L.C. Katz. Recruitment of Local Inhibitory Networks by Horizontal Connections in Layer 2/3 of Ferret Visual Cortex. *Journal of Neurophysiology*, 89(1):501–512, 2003.

[30] T.R. Tucker and L.C. Katz. Spatiotemporal Patterns of Excitation and Inhibition Evoked by the Horizontal Network in Layer 2/3 of Ferret Visual Cortex. *Journal of Neurophysiology*, 89(1):488–500, 2003.

Unité de recherche INRIA Sophia Antipolis
2004, route des Lucioles - BP 93 - 06902 Sophia Antipolis Cedex (France)

Unité de recherche INRIA Futurs : Parc Club Orsay Université - ZAC des Vignes
4, rue Jacques Monod - 91893 ORSAY Cedex (France)
Unité de recherche INRIA Lorraine : LORIA, Technopôle de Nancy-Brabois - Campus scientifique
615, rue du Jardin Botanique - BP 101 - 54602 Villers-lès-Nancy Cedex (France)
Unité de recherche INRIA Rennes : IRISA, Campus universitaire de Beaulieu - 35042 Rennes Cedex (France)
Unité de recherche INRIA Rhône-Alpes : 655, avenue de l'Europe - 38334 Montbonnot Saint-Ismier (France)
Unité de recherche INRIA Rocquencourt : Domaine de Voluceau - Rocquencourt - BP 105 - 78153 Le Chesnay Cedex (France)

Éditeur
INRIA - Domaine de Voluceau - Rocquencourt, BP 105 - 78153 Le Chesnay Cedex (France)
http://www.inria.fr
ISSN 0249-6399